Inorganic Chemistry

pubs.acs.org/IC

Article

Experimental Evidence of *syn* H−N−Fe−H Configurational Requirement for Iron-Based Bifunctional Hydrogenation Catalysts

Huiguang Dai, Weishi Li, Jeanette A. Krause, and Hairong Guan*

Cite This: *Inorg. Chem.* 2021, 60, 6521−6535

Read Online

ACCESS | Metrics & More | Article Recommendations | Supporting Information

ABSTRACT: Iron hydrides supported by a pincer ligand of the type $HN(CH_2CH_2PR_2)_2$ ($^{R}PN^{H}P$) are versatile hydrogenation catalysts. Previous efforts have focused on using CO as an additional ligand to stabilize the hydride species. In this work, CO is replaced with isocyanide ligands, leading to the isolation of two different types of iron hydride complexes: ($^{R}PN^{H}P$)FeH(CNR′)(BH_4) (R = ^{i}Pr, R′ = 2,6-$Me_2C_6H_3$, ^{t}Bu; R = Cy, R′ = 2,6-$Me_2C_6H_3$) and [($^{iPr}PN^{H}P$)FeH($CN^{t}Bu)_2$]X (X = BPh_4, Br, or a mixture of Br and BH_4). The neutral iron hydrides are capable of catalyzing the hydrogenation of $PhCO_2CH_2Ph$ to $PhCH_2OH$, although the activity is lower than for ($^{iPr}PN^{H}P$)FeH(CO)(BH_4). The cationic iron hydrides are active hydrogenation catalysts only for more reactive carbonyl substrates such as PhCHO, and only when the NH and FeH hydrogens are *syn* to each other. The cationic species and their synthetic precursors [($^{iPr}PN^{H}P$)FeBr($CN^{t}Bu)_2$]X (X = BPh_4, Br) can have different configurations for the isocyanide ligands (*cis* or *trans*) and the H−N−Fe−H(Br) unit (*syn* or *anti*). Unlike tetraphenylborate, the bromide counterion participates in a hydrogen-bonding interaction with the NH group, which influences the relative stability of the *cis,anti* and *cis,syn* isomers. These structural differences have been elucidated by X-ray crystallography, and the geometric isomerization processes have been studied by NMR spectroscopy.

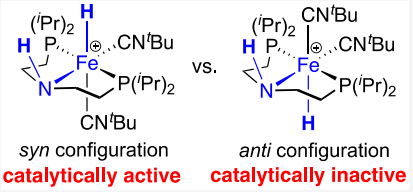

INTRODUCTION

Recent years have witnessed an upsurge of interest in developing iron-based homogeneous hydrogenation catalysts,[1] largely sparked by the fact that iron is an earth-abundant and inexpensive metal. As far as the hydrogenation of C=O bonds is concerned, this research field started to attract attention in the late 2000s, when the Knölker complex (a hydroxycyclopentadienyl iron dicarbonyl hydride)[2] was demonstrated as the first well-defined iron catalyst for aldehyde/ketone hydrogenation,[3] and diiminodiphosphine- and diaminodiphosphine-ligated iron complexes were established as the first iron-based catalytic systems for the asymmetric hydrogenation of ketones.[4] Since these early reports, a variety of iron complexes, especially those supported by a pincer ligand, have been developed for improved catalytic efficiency[5,6] and/or enantioselectivity.[7,8] In the meantime, considerable efforts have been made to apply the iron-based hydrogenation strategy to the reduction of other carbonyl-containing substrates such as CO_2/bicarbonates/carbonates,[9,10] esters,[11,12] amides,[13] and oxamides.[14]

Diphosphines bearing a central NH group that can bind metals through the [PNP] donor set are among the most successful ligands in designing iron catalysts for hydrogenation reactions.[1i,j,15] It is generally believed that an iron hydride bearing an H−N−Fe−H unit is the catalytically active species. In the Noyori-type metal−ligand bifunctional mechanism (Scheme 1, Catalytic Cycle A),[16] a concerted H^-/H^+ transfer[17] from the iron hydride to a carbonyl substrate would produce an iron amido complex. The catalytic cycle can be completed by a subsequent dihydrogen activation, which is often proposed to be facilitated by water (impurity) or an alcohol (solvent or the hydrogenation product).[17a,18] In this mechanism, the NH group is chemically noninnocent, as it participates in bond-forming and bond-breaking processes. While PNP-ligated iron amido complexes have been isolated and used to activate dihydrogen,[9b,19] computational work by Dub[17,20] and others[21] focusing on group 8 metal-based hydrogenation catalysts suggest that the energetically more favorable pathway involves a zwitterionic species or an ion-pair intermediate resulting from hydride transfer (Scheme 1, Catalytic Cycle B). This intermediate can activate dihydrogen without breaking the N−H bond. In this mechanism, the NH group is chemically innocent but cooperative, as it plays an important role of stabilizing key transition states through hydrogen-bonding interactions. The presence of alcohol molecules (as the solvent or generated from the hydrogenation reaction) can provide additional stabilization effects through a more elaborate hydrogen-bonding network.[22]

The most commonly used method to *experimentally* probe the effect of the NH group is to convert it into an *N*-alkyl group. In a number of cases,[5d,g,9c,e,g,h] the modified iron catalysts remain active, suggesting that hydrogenation steps can take place solely at the metal site without the involvement of the NH functionality.[23] Loss of catalytic activity after alkylation of the

Received: February 1, 2021
Published: April 22, 2021

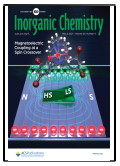

Scheme 1. Proposed Catalytic Cycles for the Hydrogenation of Carbonyl Substrates Catalyzed by H−N−Fe−H Type Complexes

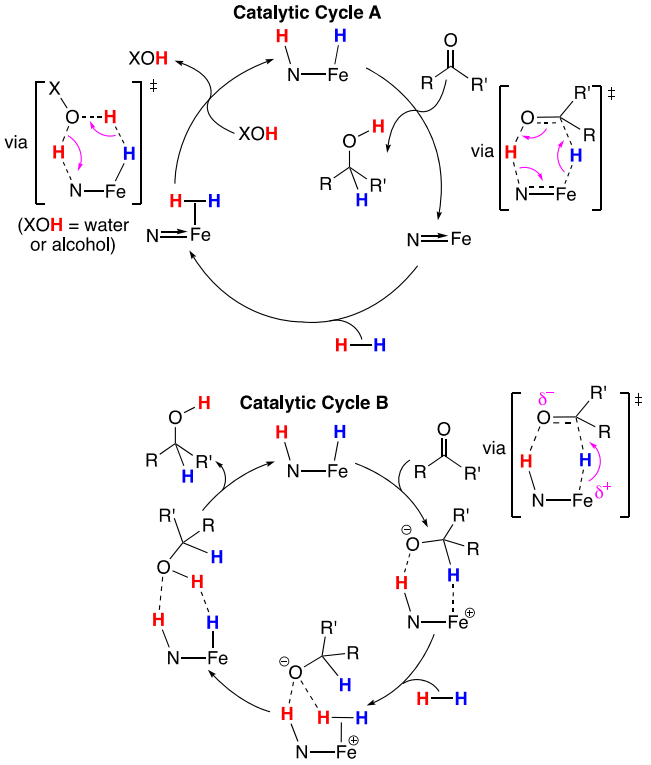

NH group, on the other hand, is often interpreted as proof for the Noyori-type metal−ligand bifunctional mechanism (Scheme 1, Catalytic Cycle A).[11b,19a,24] A more contemporary mechanistic view (Scheme 1, Catalytic Cycle B) attributes the drop in catalytic activity to two factors: (1) the removal of the hydrogen-bonding interactions that are critical to stabilizing the key transition states and (2) increased steric crowding near the hydride.[23a] One could also argue that changing NH to *N*-alkyl could simply alter the electronic and steric properties of the ligand, resulting in an inactive catalyst, even when the hydrogenation mechanism does not involve the NH functionality. Furthermore, the presence of an H−N−M−H unit does not necessarily require the NH group to be cooperative, especially when the H−N−M−H dihedral angle is relatively wide (e.g. ∼60°).[25] Alkylation of these catalysts could be beneficial due to improved catalyst stability.[23a] Nevertheless, if hydrogen-bonding interactions with the NH group are indeed required during the iron-catalyzed hydrogenation reactions, the two hydrogens in the H−N−Fe−H unit must be spatially arranged such that the NH functionality is within the reach of the oxygen atom after hydride transfer. It is thus important to study the correlation between the catalytic activity and H−N−Fe−H type complexes with different hydrogen configurations.

We have been interested in developing iron-based catalysts for the hydrogenation of esters, including the industrially relevant fatty acid methyl esters.[11d] In 2014, the Beller group[11b,e] and our group[11c] independently reported that $HN(CH_2CH_2PR_2)_2$-ligated iron hydrido borohydride complexes (Scheme 2) were effective in catalyzing ester hydrogenation. In attempts to improve the catalytic system, we set out to replace CO in the original catalysts with isocyanides, considering that such ligands are tunable and, like CO, can force the metal to adopt a low-spin

Scheme 2. Original Ester Hydrogenation Catalysts and the Isocyanide Derivatives

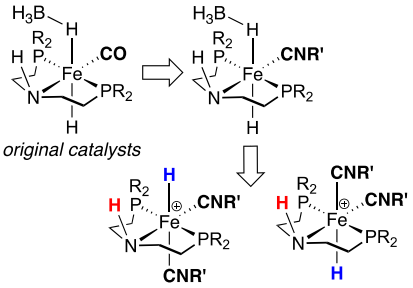

state.[26] During the synthesis of the corresponding hydrido borohydride complexes, we encountered cationic bis-(isocyanide) complexes in which the lone hydride ligand can be *syn* or *anti* to the NH hydrogen (Scheme 2). These configurational isomers are separable, providing a rare opportunity to study the structure−reactivity relationship in the context of metal−ligand bifunctional catalysis. The key finding, along with the catalytic study of the neutral hydrido borohydride complexes (benchmarked to the original catalysts), is reported in this paper.

RESULTS AND DISCUSSION

Synthesis of Iron Hydrido Borohydride Complexes. In studying the catalytic hydrogenation of CO_2 to formate, Bernskoetter, Hazari, and co-workers developed a two-step synthesis of (^{iPr}PN^{H}P)FeH(CNAr)(BH_4) (**1**, Ar = 2,6-dimethylphenyl) starting from the PNP pincer ligand[27] $HN(CH_2CH_2P^iPr_2)_2$ (abbreviated as ^{iPr}PN^{H}P) and $FeCl_2$ (Scheme 3).[9f] To ensure that only one molecule of the isocyanide ligand binds to iron, slow addition of a dilute ligand solution to the *in situ* generated (^{iPr}PN^{H}P)$FeCl_2$ was needed. We modified the procedure slightly by cooling the reaction mixture to 0 °C prior to dropwise addition of the isocyanide and performing the subsequent reaction with $NaBH_4$ in the same reaction vessel. This one-pot protocol was convenient and was also effective for incorporating only 1 equiv of an alkyl isocyanide such as *tert*-butyl isocyanide (CN^tBu), which previously was reported to be problematic.[9f] With the new method, (^{iPr}PN^{H}P)FeH(CN^tBu)(BH_4) (**2**) and the cyclohexyl analogue of **1**, (^{Cy}PN^{H}P)FeH(CNAr)(BH_4) (**3**), were isolated as yellow powders in 46% and 45% overall yields, respectively.

The presence of hydride ligands in **2** and **3** was confirmed by NMR and IR spectroscopy. The ^{1}H NMR spectra (in C_6D_6) feature a triplet in the upfield region (**2**, −21.80 ppm, J_{P-H} = 52.7 Hz; **3**, −21.23 ppm, J_{P-H} = 52.8 Hz) attributed to the terminal hydride on iron and a very broad signal centered around −3.06 ppm (integrates to 4H), which can be assigned to the BH_4 resonance. The IR spectra of the solid samples display an Fe−H stretching vibration (**2**, 1782 cm^{-1}; **3**, 1835 cm^{-1}) and multiple B−H stretching vibrations (**2**, 2339, 2327, 2296 cm^{-1}; **3**, 2341, 2325, 2032 cm^{-1}). The frequencies and the number of B−H stretching bands support a monodentate BH_4 ligand[28] with the possibility of forming an intramolecular dihydrogen bond with the NH group (i.e., $N-H^{\delta+}\cdots^{\delta-}H-B$).[29] As is expected for isocyanide complexes, the IR spectra also show a very intense C≡N stretching vibration (**2**, 2000 cm^{-1}; **3**, 1973 cm^{-1}). Overall, these diagnostic NMR and IR data are similar to those reported for **1**[9f] as well as those for the analogous carbonyl complexes (^{R}PN^{H}P)FeH(CO)(BH_4).[7h,11c,e,13b,c,30]

https://doi.org/10.1021/acs.inorgchem.1c00328
Inorg. Chem. 2021, 60, 6521−6535

Scheme 3. Synthetic Route to the Neutral Iron Hydrido Borohydride Complexes

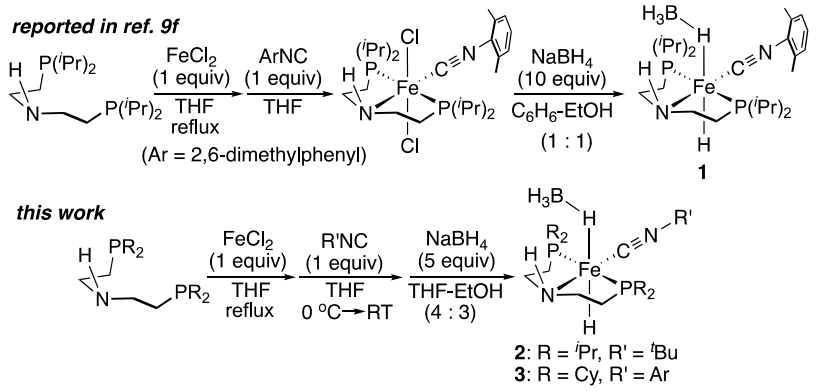

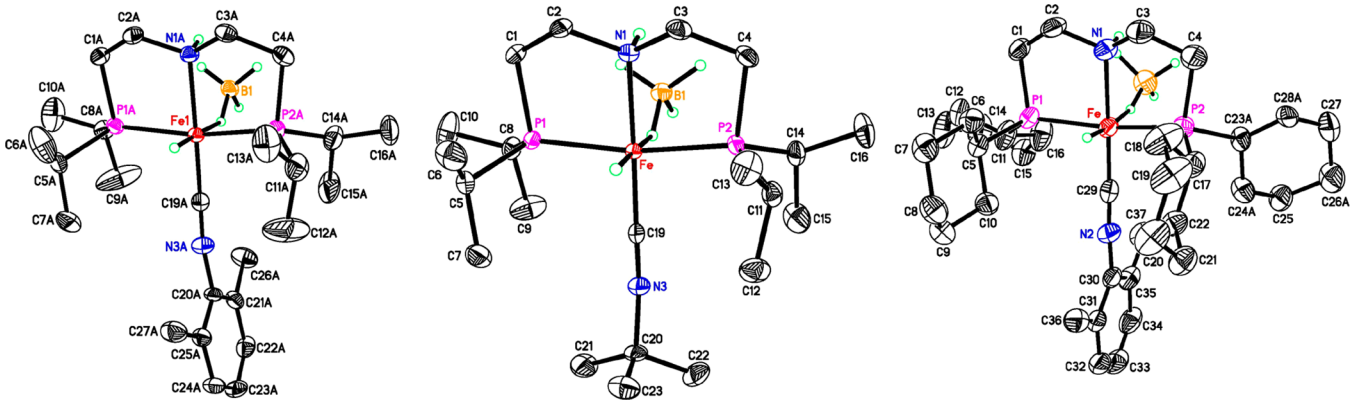

Figure 1. ORTEP drawings of one of the independent molecules of (^{iPr}PN^{H}P)FeH(CNAr)(BH$_4$) (**1**, left), (^{iPr}PN^{H}P)FeH(CN^{t}Bu)(BH$_4$) (**2**, center), and (^{Cy}PN^{H}P)FeH(CNAr)(BH$_4$) (**3**, right) at the 50% probability level. All hydrogen atoms except the those bound to nitrogen, boron, and iron are omitted for clarity.[31]

The structures of the iron hydrido borohydride complexes, including the previously known compound **1**, were further studied by X-ray crystallography. As illustrated in Figure 1, iron is situated in an octahedral coordination environment with a monodentate BH$_4$ ligand *trans* to a hydride. Of the three terminal hydrogens bound to boron, two have close contacts with the NH hydrogen (H$^{\delta+}$···$^{\delta-}$H distance: 2.11−2.40 Å). This phenomenon was observed previously for (^{iPr}PN^{H}P)FeH(CO)(BH$_4$) and explained by a bifurcated intramolecular dihydrogen bond.[30b] Like (^{iPr}PN^{H}P)FeH(CO)(BH$_4$), **1** and **2** also pack in the crystal lattice with a pair of molecules linked by intermolecular N−H$^{\delta+}$···$^{\delta-}$H−B dihydrogen bonds (H$^{\delta+}$···$^{\delta-}$H distance: 2.40−2.79 Å). In contrast, **3** shows a completely different 3-D network without these types of Coulombic interactions, presumably because of the steric bulk of the cyclohexyl groups. A comparison of the key bond distances and angles suggests minimal perturbation of the structure stemming from the isocyanide ligand and phosphorus substituents. The only marked difference is the isocyanide C≡N−C angle, which shows a greater deviation from linearity for the *tert*-butyl isocyanide complex (**2**, 165.76(11)°) in comparison to the aryl isocyanide derivatives (**1**, 171.3(4), 173.7(4)°; **3**, 170.0(3)°).

Synthesis of Cationic Iron Bis(isocyanide) Bromide Complexes. Alkyl isocyanides have the tendency to displace a chloride ligand in (^{iPr}PN^{H}P)FeCl$_2$ to form cationic bis(isocyanide) complexes, especially when the reaction is carried out at room temperature. The study by Bernskoetter, Hazari, and co-workers showed that mixing ^{iPr}PN^{H}P, FeCl$_2$, and CN^{i}Pr in a 1:1:1 ratio produced [(^{iPr}PN^{H}P)FeCl(CN^{i}Pr)$_2$]$_2$[FeCl$_4$].[9f] A similar result was obtained during our initial effort to make (^{iPr}PN^{H}P)FeBr$_2$(CN^{t}Bu) from ^{iPr}PN^{H}P, FeBr$_2$, and CN^{t}Bu. Doubling the amount of CN^{t}Bu, however, led to the isolation of a green powder identified as a 45:55 mixture[32,33] of *trans* and *cis,anti* isomers of [(^{iPr}PN^{H}P)FeBr(CN^{t}Bu)$_2$]Br (**4**) with a combined yield of 78% (Scheme 4). Attempts to separate the

Scheme 4. Synthesis of [(^{iPr}PN^{H}P)FeBr(CN^{t}Bu)$_2$]Br (4)

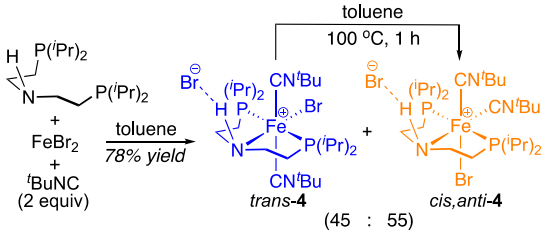

two isomers via recrystallization were unsuccessful. The *trans* isomer is a kinetic product. At room temperature, the ratio of the two isomers remained unchanged over a prolonged period of time. However, when the isomeric mixture in toluene was kept at 100 °C for 1 h, a complete isomerization of *trans*-**4** to *cis,anti*-**4** was observed, which allowed pure *cis,anti*-**4** to be isolated in 74% yield as a yellow powder. The *cis,anti* isomer is thermodynamically more stable, presumably because the two strongly *trans* influencing isocyanide ligands can avoid being *trans* to each other.

https://doi.org/10.1021/acs.inorgchem.1c00328
Inorg. Chem. 2021, 60, 6521−6535

The bromide counterion in both isomers forms a hydrogen bond with the NH group. For the isomeric mixture dissolved in C_6D_6, the N*H* resonances of *trans*-**4** and *cis,anti*-**4** appear at 5.23 and 7.80 ppm, respectively, consistent with N−H···Br bonding interactions.[34] The presence of a hydrogen bond is further supported by a very broad N−H stretching band (~3350 cm^{-1}) found in the IR spectra and, in the case of *cis,anti*-**4**, confirmed by X-ray crystallography (Figure 2). The crystallographic study also

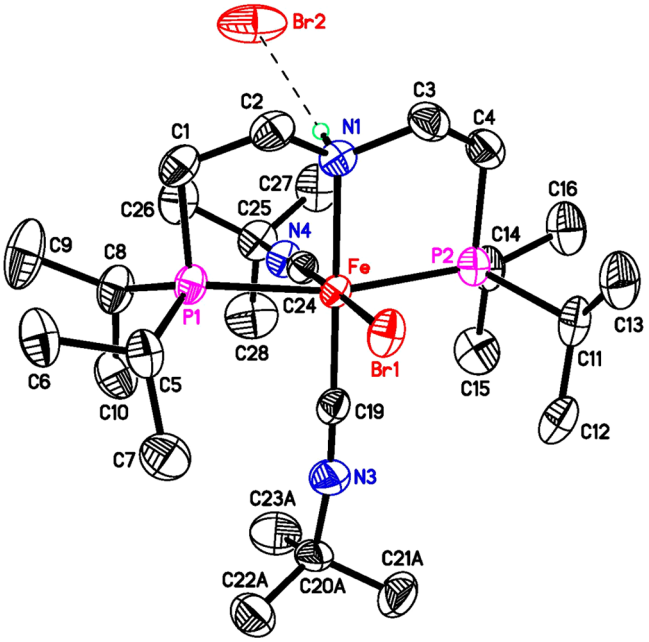

Figure 2. ORTEP drawing of *cis,anti*-[(^{iPr}PN^{H}P)FeBr(CN^{t}Bu)$_2$]Br·1/2C_7H_8 (*cis,anti*-**4**·1/2C_7H_8) at the 50% probability level. A cocrystallized half-molecule of toluene and all hydrogen atoms except that bound to nitrogen are omitted for clarity.[36]

establishes the *anti* configuration of the NH hydrogen in relation to the covalently bonded bromide. This *anti* configuration is similarly favored in [(^{iPr}PN^{H}P)FeCl(CNAr)$_2$]Cl[9f] and-[(^{Ph}PN^{H}P)RuCl(NCMe)(NHC)]Cl (NHC = 1,3-dimethylimidazol-2-ylidene),[35] presumably to minimize the electrostatic repulsion between the two halides.

The hydrogen bond can be disrupted by performing an anion exchange reaction with $NaBPh_4$ (Scheme 5), a process that does not appear to erode the stereochemistry. Thus, *cis,anti*-**4** was cleanly converted to *cis,anti*-[(^{iPr}PN^{H}P)FeBr(CN^{t}Bu)$_2$]BPh_4 (*cis,anti*-**5**), and a 42:58 mixture of *trans*-**4** and *cis,anti*-**4** was converted to a mixture of *trans*-**5** and *cis,anti*-**5** and isolated in a 47:53 ratio as determined by NMR. The use of tetraphenylborate as the counterion made the cationic complexes crystallize more readily. When the mixture of *trans*-**5** and *cis,anti*-**5** in THF (a green solution) layered with EtOH was kept at −30 °C, blue crystals formed within 1 day. Though the recovery yield was low (15% based on the total mass), the isolated blue compound was predominantly *trans*-**5** (97% purity).

For a crystallographic study, the mixture of *trans*-**5** and *cis,anti*-**5** was first dissolved in MeCN and then layered with EtOH. Both blue−purple and yellow−orange dichroic crystals were obtained from this sample, indicating that the green solution is a mixture of blue and yellow. The blue−purple dichroic crystals were proven to be *trans*-**5**, with the cation being shown in Figure 3. Interestingly, the yellow−orange dichroic crystals were shown to be an acetonitrile complex, *cis*-[(^{iPr}PN^{H}P)Fe(NCMe)(CN^{t}Bu)$_2$][BPh_4]$_2$ (*cis*-**6**) (see the Supporting Information for details), which likely resulted from ligand substitution with *cis,anti*-**5**. The bromide in *trans*-**5** is clearly less labile, consistent with a weaker *trans* effect of the opposing ligand (i.e. the NH group). With the isomeric mixture as the starting material, single crystals were also grown from THF−Et_2O to avoid the complication of solvent coordination. The resulting blue−purple and yellow−orange dichroic crystals were identified as *trans*-**5** and *cis,anti*-**5**, respectively (Figure 3).

The Fe−Br bond in *cis,anti* -**5** (2.5227(4) Å) is longer than that in *trans*-**5** (2.4956(6) Å), as determined by X-ray crystallography. Similarly, the *trans*-effect argument can be used to explain a comparably long Fe−N bond observed for *cis,anti*-**5** (2.0837(19) Å vs 2.064(3) Å in *trans*-**5**) and two elongated iron−isocyanide bonds noted for *trans*-**5** (1.856(4) and 1.885(4) Å vs 1.817(2) and 1.834(3) Å in *cis,anti*-**5**). The remaining metrical details are virtually indistinguishable between the two isomers. Comparing *cis,anti*-**4** with *cis,anti*-**5** suggests that the hydrogen bond has little effect on the bonding environment about the iron, only causing a minor 0.01−0.03 Å contraction of the Fe−N and Fe−Br bond distances.

Scheme 5. Synthesis of [(^{iPr}PN^{H}P)FeBr(CN^{t}Bu)$_2$]BPh_4 (5) as the Pure *cis,anti* or *trans* Isomer

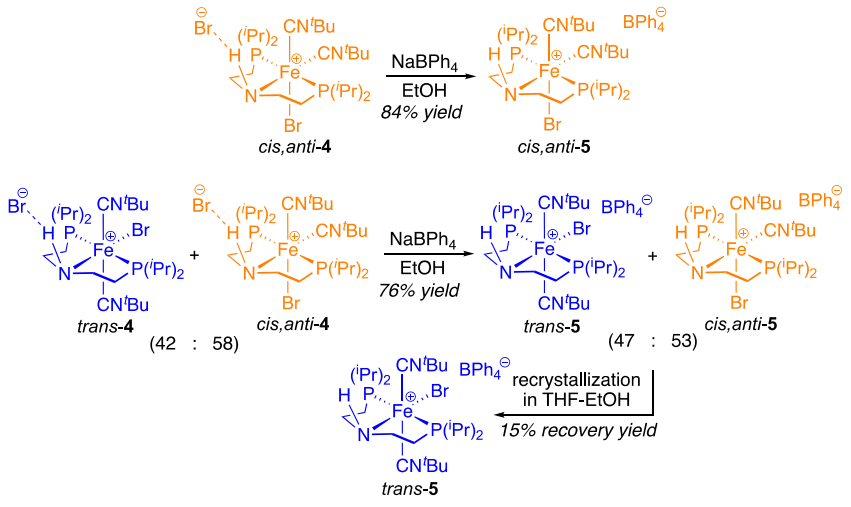

https://doi.org/10.1021/acs.inorgchem.1c00328
Inorg. Chem. 2021, 60, 6521−6535

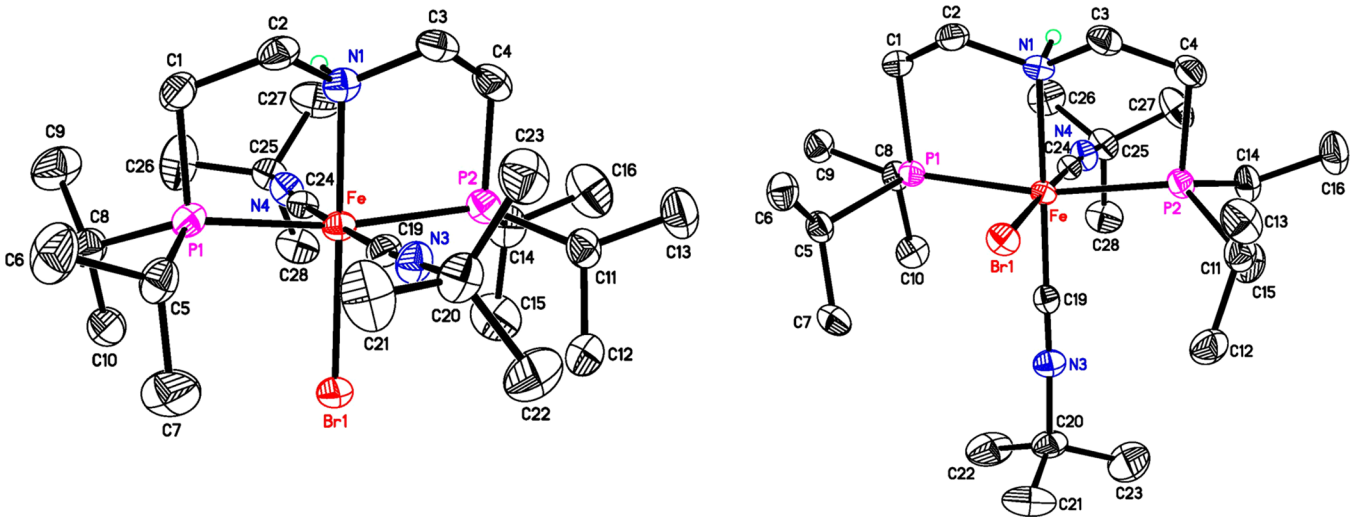

Figure 3. ORTEP drawings of the cations in *trans*-[(^{iPr}PN^{H}P)FeBr(CN^{t}Bu)$_2$]BPh$_4$·MeCN (*trans*-**5**·MeCN, left) and *cis,anti*-[(^{iPr}PN^{H}P)FeBr(CN^{t}Bu)$_2$]BPh$_4$·2THF (*cis,anti*-**5**·2THF, right) at the 50% probability level. All hydrogen atoms except that bound to nitrogen are omitted for clarity.

The two isomers of **5** can be readily differentiated by NMR spectroscopy. In particular, the N*H* resonance of *trans*-**5** (in CD_2Cl_2) is significantly shielded, displaying a triplet at −0.52 ppm (J = 7.6 Hz). The corresponding resonance in *cis,anti*-**5** is located at 2.39 ppm also as a triplet (J = 12.0 Hz). It is not surprising that these chemical shift values are much lower than those for *trans*-**4** and *cis,anti*-**4**, in which an N−H···Br hydrogen bond is involved. The ^{31}P{^{1}H} NMR spectra show that *trans*-**5** (56.7 ppm) differs from *cis,anti*-**5** (68.7 ppm) by 12 ppm, similar to the trend observed with *trans*-**4** (59.1 ppm) and *cis,anti*-**4** (71.2 ppm). The lack of a hydrogen bond in *trans*-**5** and *cis,anti*-**5** is further confirmed by relatively sharp N−H stretching bands at 3235 and 3229 cm^{-1}, respectively. *trans*-**5** exhibits only one very intense C≡N stretching band at 2102 cm^{-1}, although its NMR spectra support the presence of two inequivalent isocyanide ligands. In contrast, *cis,anti*-**5** has two distinct IR bands at 2134 and 2086 cm^{-1} attributed to the C≡N stretch.

Given the isomerization from *trans*-**4** to *cis,anti*-**4** (Scheme 4), we anticipated that *trans*-**5** would be thermodynamically less stable than *cis,anti*-**5**. The geometric isomerization process was studied in chlorobenzene (Scheme 6) due to solubility and boiling point considerations. Heating a 47:53 mixture of *trans*-**5** and *cis,anti*-**5** at 100 °C for 18 h led to the disappearance of *trans*-**5** but surprisingly yielded a third isomer along with *cis,anti*-**5** in a 91:9 ratio. An identical result was obtained when pure *trans*-**5** or *cis,anti*-**5** was employed. This new isomer, recrystallized from THF−Et_2O, was identified by X-ray crystallography as *cis,syn*-**5** (Figure 4). Under the isomerization conditions (100 °C, 18 h), pure *cis,syn*-**5** can revert back to the 91:9 mixture of *cis,syn*-**5** and *cis,anti*-**5**, suggesting that this ratio reflects the thermodynamic stability of these two isomers. Without the hydrogen-bonded bromide, *cis,syn*-**5** becomes the most stable isomer, likely due to a weak but favorable dipole−dipole interaction between $N^{\delta-}$−$H^{\delta+}$ and $Fe^{\delta+}$−$Br^{\delta-}$.

In comparison to *cis,anti*-**5**, *cis,syn*-**5** features a shorter Fe−N bond (2.0597(14) vs 2.0837(19) Å) and a shorter Fe−Br bond (2.4993(3) vs 2.5227(4) Å), possibly a consequence of the aforementioned dipole−dipole interaction. The C≡N−C angle of the CN^{t}Bu ligand *trans* to the NH group is bent slightly (169.94(18)°) compared to the other CN^{t}Bu ligands for the three isomers reported here (175.9(3)-177.8(4)°). The bent C≡N−C angle is often an indication of increased back-donation from metal to the isocyanide π^* orbital,[38] although the C≡N stretching bands of *cis,syn*-**5** (2129 and 2090 cm^{-1}) do not necessarily appear at wavenumbers lower than those of *cis,anti*-**5** (2134 and 2086 cm^{-1}). For cationic complexes, the differences in $\nu_{C\equiv N}$ values likely reflect electrostatic effects rather than the extent of back-donation.[39] The IR spectrum of *cis,syn*-**5** also shows an N−H stretching band at 3198 cm^{-1}, which is 31 and 37 cm^{-1} lower than for *cis,anti*-**5** and *trans*-**5**, respectively, suggesting a weaker N−H bond. The N*H* resonance of *cis,syn*-**5** (in CD_2Cl_2) cannot be precisely located due to overlap with the NCH_2 resonances but is definitely in the more downfield region (3.33−2.90 ppm) in comparison to *cis,anti*-**5** and *trans*-**5**. The phosphorus resonance of *cis,syn*-**5** (71.2 ppm) is distinguishable from those of *cis,anti*-**5** (68.7 ppm) and *trans*-**5** (56.7 ppm) and is shifted downfield the most among the three isomers.

Scheme 6. Geometric Isomerization of [(^{iPr}PN^{H}P)FeBr(CN^{t}Bu)$_2$]BPh$_4$ (5)

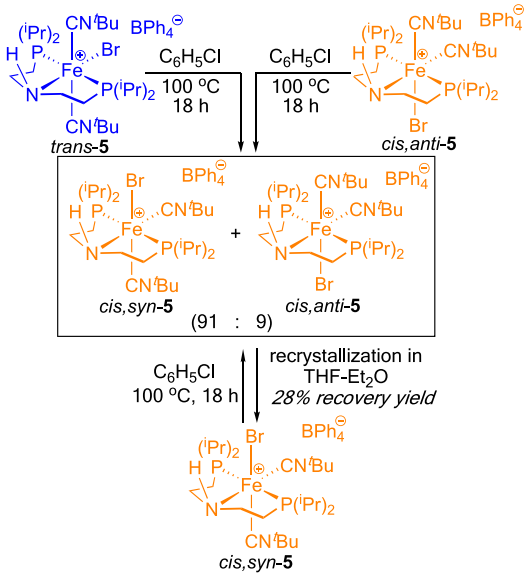

Synthesis of Cationic Iron Bis(isocyanide) Hydride Complexes. To synthesize the iron hydride complexes, a 45:55

https://doi.org/10.1021/acs.inorgchem.1c00328
Inorg. Chem. 2021, 60, 6521−6535

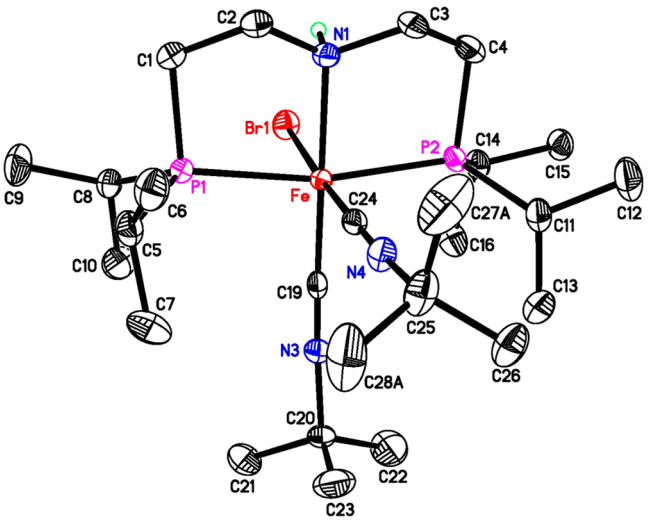

Figure 4. ORTEP drawing of the cation in *cis,syn*-$[(^{iPr}PN^{H}P)FeBr(CN^{t}Bu)_2]BPh_4$ (*cis,syn*-**5**) at the 50% probability level. All hydrogen atoms except that bound to nitrogen are omitted for clarity.[37]

mixture of *trans*-**4** and *cis,anti*-**4** was treated with 5 equiv of $NaBH_4$ in EtOH and then heated at 50 °C for 16 h (Scheme 7).

Scheme 7. Synthesis of *cis,anti*-$[(^{iPr}PN^{H}P)FeH(CN^{t}Bu)_2]BPh_4$ (*cis,anti*-8**)**

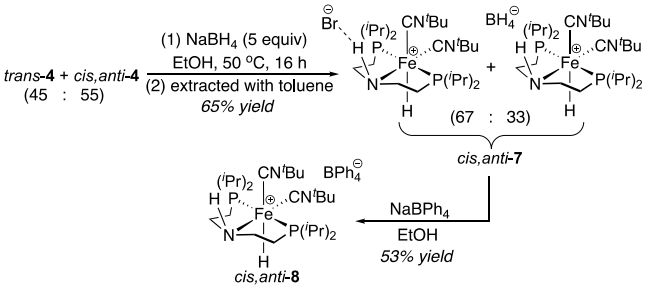

Subsequent removal of the solvent followed by extraction with toluene led to the isolation of *cis,anti*-$[(^{iPr}PN^{H}P)FeH(CN^{t}Bu)_2]X$ (*cis,anti*-**7**, X = mixed anion) in 65% yield. On the basis of ^1H NMR and elemental analysis, the cation is paired with 67% Br^- and 33% BH_4^-. Once again, the bromide must be hydrogen-bonded to the NH group, as suggested by a downfield-shifted N*H* resonance (6.40 ppm, in C_6D_6). The borohydride is expected to have a weaker, if any, interaction with the NH group. The B*H*$_4$ resonance appears as a sharp quartet at 0.97 ppm (J_{B-H} = 81.3 Hz), consistent with a high symmetry for the quadrupolar nucleus ^{11}B. The observation of two B−H stretching bands (for a solid sample) at 2285 and 2214 cm^{-1} also implies no significant elongation or contraction of B−H bonds from the free BH_4^-.[28c] Both Br^- and BH_4^- in *cis,anti*-**7** can be replaced by BPh_4^- following an anion exchange reaction with $NaBPh_4$, allowing *cis,anti*-$[(^{iPr}PN^{H}P)FeH(CN^{t}Bu)_2]BPh_4$ (*cis,anti*-**8**) to be isolated as a white powder.

The toluene extraction step (i.e., step (2) in Scheme 7) is key to obtaining a pure *cis,anti* isomer.[40] The residue left after EtOH evaporation was redissolved in CD_3OD and analyzed as a 28:72 mixture, favoring a new isomer. This result suggests that isomerization occurred during the workup. In fact, adding $NaBPh_4$ directly to the reaction mixture in EtOH (after the $NaBH_4$ reaction was complete) yielded a white precipitate, which proved to be a 32:68 mixture of *cis,anti*-**8** and *cis,syn*-**8** (Scheme 8). Recrystallization of this mixture from THF−EtOH provided *cis,syn*-**8** as a white solid with 98% purity.

Scheme 8. Synthesis of *cis,syn*-$[(^{iPr}PN^{H}P)FeH(CN^{t}Bu)_2]BPh_4$ (*cis,syn*-8**)**

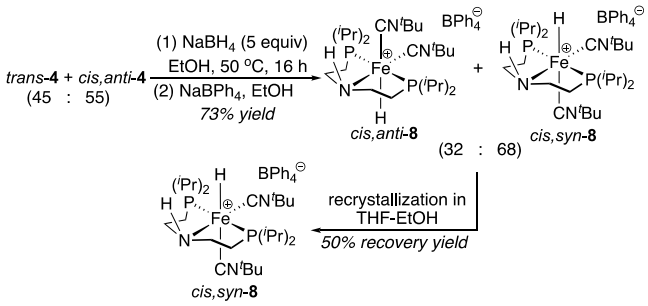

Single crystals of *cis,anti*-**8** and *cis,syn*-**8** were grown separately by starting with the purified isomers. Both nitrogen- and iron-bound hydrogens were located directly from the difference map, confirming the proposed stereochemistry (Figure 5). A structural comparison shows that the Fe−N bond is shorter in *cis,syn*-**8** (2.0837(13) Å) than in *cis,anti*-**8** (2.104(3) Å), analogous to the trend seen with the bromide complexes *cis,syn*-**5** and *cis,anti*-**5**. Similarly, *cis,syn*-**8** adopts a more bent C≡N−C angle for the CN*t*Bu ligand *trans* to the NH group (170.45(7)°) relative to others in this series. Replacing the bromide with a hydride (isomers **5** → isomers **8**) results in two major structural changes: (1) the Fe−P bonds are shortened by ∼0.07 Å, and (2) the two Fe−C bond distances in each isomer differ by ∼0.05 Å due to the *trans* effect (the Fe−C bond *trans* to the hydride is longer).

Unlike *cis,anti*-**7**, both *cis,anti*-**8** and *cis,syn*-**8** dissolve poorly in C_6D_6; therefore, CD_3CN was used for the NMR analysis. The ^1H NMR spectrum of *cis,anti*-**8** shows a triplet at −10.28 ppm (J_{P-H} = 51.6 Hz) characteristic of a hydride and a multiplet at 3.08−2.96 ppm consistent with an N*H* resonance devoid of a hydrogen-bonding interaction. The hydride resonance of *cis,syn*-**8** is also a triplet but is shifted to −9.75 ppm (J_{P-H} = 53.2 Hz). The corresponding N*H* resonance is overlapped with other resonances in the 2.88−2.70 ppm range. The ^{31}P chemical shift values for *cis,anti*-**8** (100.7 ppm) and *cis,syn*-**8** (103.4 ppm) follow a trend similar to that for *cis,anti*-**5** (68.7 ppm) and *cis,syn*-**5** (71.2 ppm). It is worth noting that these phosphorus NMR signals are insensitive to the solvent employed and are particularly useful for analyzing the isomeric ratio.

At room temperature, *cis,anti*-**8** and *cis,syn*-**8** in their pure form are configurationally stable. *cis,syn*-**8** is likely thermodynamically more stable than *cis,anti*-**8** because of the favorable dipole−dipole interaction between $N^{\delta-}-H^{\delta+}$ and $Fe^{\delta+}-H^{\delta-}$. As in the case of **4** and **5**, the relative stability can be reversed when a hydrogen-bonded bromide is involved. The reaction of *trans*-**4** and *cis,anti*-**4** with $NaBH_4$ was carried out in EtOH (or analyzed in CD_3OD) to determine whether the disruption of the N−H···Br hydrogen bond by an alcoholic solvent would result in the *cis,syn* isomer as the major product, and indeed it does. Rapid precipitation induced by the addition of $NaBPh_4$ essentially takes a snapshot of the isomeric ratio (Scheme 8). Removal of EtOH from the solution containing the initial products should restore the N−H···Br hydrogen bond, leading to the isolation of the *cis,anti* isomer as long as a nonalcoholic solvent such as toluene is used for extraction (Scheme 7). However, this still

https://doi.org/10.1021/acs.inorgchem.1c00328
Inorg. Chem. 2021, 60, 6521−6535

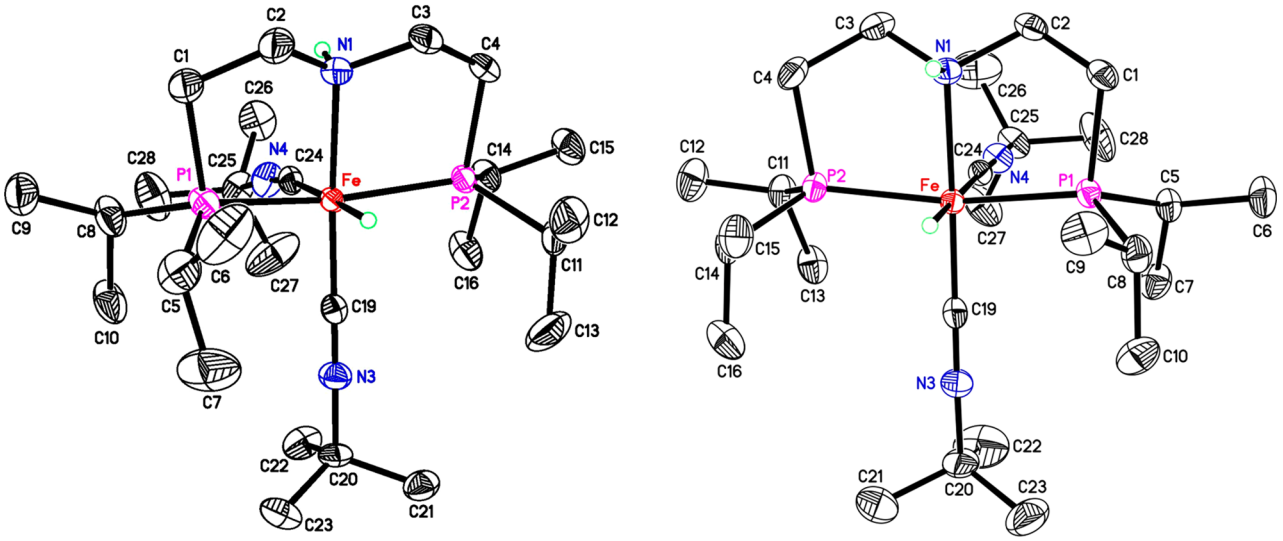

Figure 5. ORTEP drawings of the cations in *cis,anti*-[(^{iPr}PN^{H}P)FeH(CN^{t}Bu)$_2$]BPh$_4$ (*cis,anti*-**8**, left) and *cis,syn*-[(^{iPr}PN^{H}P)FeH(CN^{t}Bu)$_2$]BPh$_4$ (*cis,syn*-**8**, right) at the 50% probability level. All hydrogen atoms except those bound to nitrogen and iron are omitted for clarity.

requires a *cis,syn* to *cis,anti* isomerization process. In principle, the NH group could dissociate from iron, followed by an inversion of the nitrogen lone pair and recoordination to iron to complete the isomerization. We favor an alternative mechanism involving deprotonation/reprotonation of the NH group,[41] which may be promoted by $NaBH_4$ or its alcoholysis products. To test this hypothesis, a stoichiometric amount of $NaBH_4$ was used to convert the mixture of *trans*-**4** and *cis,anti*-**4** to an iron hydride (Scheme 9), which after toluene extraction was isolated

Scheme 9. Effect of Excess $NaBH_4$ on the Isomerization Process

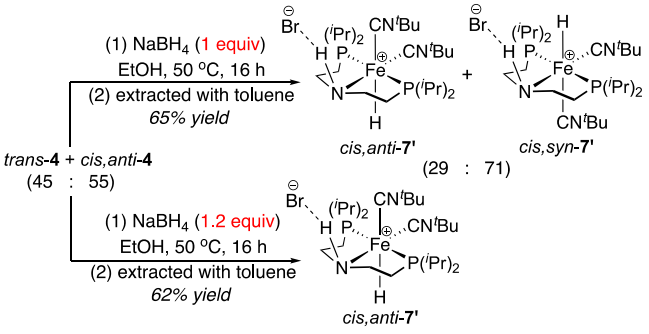

as a 29:71 isomeric mixture of [(^{iPr}PN^{H}P)FeH(CN^{t}Bu)$_2$]Br (**7′**) favoring the *cis,syn* isomer. In contrast, using 1.2 equiv of $NaBH_4$ led to the isolation of only *cis,anti*-**7′**; the structure was confirmed by X-ray crystallography (Figure 6). These results support the idea that excess $NaBH_4$ plays a crucial role in facilitating the isomerization process.

Catalytic Studies. The neutral hydrido borohydride complexes **1**−**3** and the cationic bis(isocyanide) hydride complexes *cis,anti*-**7**, *cis,anti*-**7′**, *cis,anti*-**8**, and *cis,syn*-**8** were tested as catalysts for the hydrogenation of $PhCO_2CH_2Ph$ (Table 1). For comparison purposes, the catalytic conditions were deliberately chosen so that in THF our original catalyst (^{iPr}PN^{H}P)FeH(CO)(BH$_4$) would hydrogenate only ∼50% of the substrate (entry 1). Evidently, the neutral isocyanide-ligated iron hydrides **1**−**3** (entries 4, 7, and 8) are less active than the carbonyl derivative, reducing only 10−13% of $PhCO_2CH_2Ph$ to

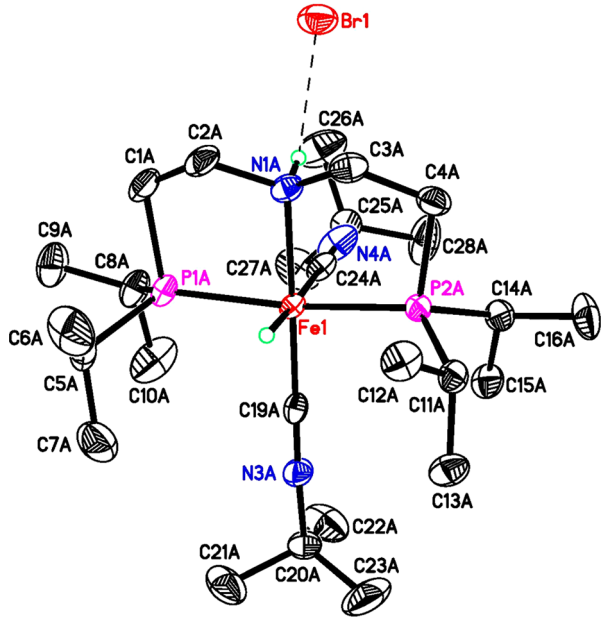

Figure 6. ORTEP drawing of one of the two independent molecules of *cis,anti*-[(^{iPr}PN^{H}P)FeH(CN^{t}Bu)$_2$]Br·1/2H$_2$O (*cis,anti*-**7′**·1/2H$_2$O) at the 50% probability level. The cocrystallized water molecule and all hydrogen atoms except those bound to nitrogen and iron are omitted for clarity.[42]

$PhCH_2OH$. These results are in alignment with previous studies of iron-catalyzed hydrogenation of CO_2 to formate, where (^{iPr}PNP)FeH(CNAr) (^{iPr}PNP= [N(CH$_2$CH$_2$P^{i}Pr$_2$)$_2$]$^-$)[9f] and (^{iPr}PN^{Me}P)FeH(CNR)(BH$_4$) (^{iPr}PN^{Me}P= MeN(CH$_2$CH$_2$P^{i}Pr$_2$)$_2$)[9g] are also outperformed by the corresponding CO-based catalysts. In the presence of 20 mol % of KO^{t}Bu, the iron catalysts (^{iPr}PN^{H}P)FeH(CO)(BH$_4$) and **1** are less effective, giving $PhCH_2OH$ with a lower yield (entries 2 and 5). A similar observation has been made by Beller and co-workers in their study of the hydrogenation of methyl benzoate catalyzed by (^{iPr}PN^{H}P)FeH(CO)(BH$_4$).[11b] In EtOH, (^{iPr}PN^{H}P)FeH(CO)(BH$_4$) and **1** are also less efficient as ester hydrogenation catalysts, in part due to the competing transesterification of

https://doi.org/10.1021/acs.inorgchem.1c00328
Inorg. Chem. 2021, 60, 6521−6535

Table 1. Hydrogenation of Benzyl Benzoate Catalyzed by the Iron Hydrides[a]

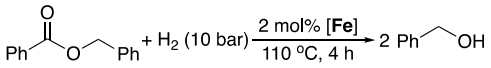

Entry	[Fe]	Solvent	Base Additive	Conversion[b]	Yield[b,c]
1	(^{iPr}PN^{H}P)FeH(CO)(BH$_4$)	THF	none	46	45
2	(^{iPr}PN^{H}P)FeH(CO)(BH$_4$)	THF	20 mol% KO^{t}Bu	38	36
3	(^{iPr}PN^{H}P)FeH(CO)(BH$_4$)	EtOH	none	44	36(7)
4	**1**	THF	none	13	13
5	**1**	THF	20 mol% KO^{t}Bu	11	10
6	**1**	EtOH	none	75	1(73)
7	**2**	THF	none	10	9
8	**3**	THF	none	13	13
9	*cis,anti*-**7**	THF	none	0	0
10	*cis,anti*-**7'**	THF	none	1	<1
11	*cis,anti*-**7'**	THF	20 mol% KO^{t}Bu	4	4
12	*cis,anti*-**7'**	EtOH	none	8	0(8)
13	*cis,anti*-**8**	THF	none	0	0
14	*cis,anti*-**8**	EtOH	none	14	0(12)
15	*cis,anti*-**8**	EtOH	20 mol% NaOEt	87	12(74)
16	*cis,syn*-**8**	THF	none	0	0
17	32% *cis,anti*-**8** + 68% *cis,syn*-**8**	THF	none	0	0
18	32% *cis,anti*-**8** + 68% *cis,syn*-**8**	THF	20 mol% KO^{t}Bu	3	3
19	32% *cis,anti*-**8** + 68% *cis,syn*-**8**	EtOH	none	40	0(38)
20	32% *cis,anti*-**8** + 68% *cis,syn*-**8**	EtOH	20 mol% NaOEt	87	11(74)

[a]Standard conditions: PhCO$_2$CH$_2$Ph (1.0 mmol), PhCH$_2$CH$_2$Ph (0.50 mmol, internal standard), and an iron catalyst (0.020 mmol) in 0.5 mL of solvent; **1** = (^{iPr}PN^{H}P)FeH(CNAr)(BH$_4$) (Ar = 2,6-dimethylphenyl), **2** = (^{iPr}PN^{H}P)FeH(CN^{t}Bu)(BH$_4$), **3** = (^{Cy}PN^{H}P)FeH(CNAr)(BH$_4$), *cis,anti*-**7** = *cis,anti*-[(^{iPr}PN^{H}P)FeH(CN^{t}Bu)$_2$]X (X = 67% Br and 33% BH$_4$), *cis,anti*-**7′** = *cis,anti*-[(^{iPr}PN^{H}P)FeH(CN^{t}Bu)$_2$]Br, *cis,anti*-**8** = *cis,anti*-[(^{iPr}PN^{H}P)FeH(CN^{t}Bu)$_2$]BPh$_4$, and *cis,syn*-**8** = *cis,syn*-[(^{iPr}PN^{H}P)FeH(CN^{t}Bu)$_2$]BPh$_4$. [b]Determined by ^{1}H NMR spectroscopy. [c]Values in parentheses are the yields of PhCH$_2$OH resulting from transesterification.

PhCO$_2$CH$_2$Ph to PhCO$_2$Et (entries 3 and 6). In fact, with **1** in EtOH, the hydrogenation process is almost completely suppressed.

In THF, the cationic iron hydrides prove to be inactive catalysts for ester hydrogenation (Table 1, entries 9, 10, 13, 16, and 17), possibly due to reduced Fe−H hydricity rendered by the positive charge of the complex. The addition of a strong base could potentially deprotonate the NH group while it converts the cationic iron hydrides to the neutral hydride (^{iPr}PNP)FeH(CN^{t}Bu)$_2$, which is expected to be more hydridic. Furthermore, studies of neutral ruthenium complexes have shown that an NH to NK conversion through the addition of KO^{t}Bu can accelerate the hydrogenation of carbonyl substrates, where the NK moiety can lower the activation barriers for the key steps.[20b,43] Our results (entries 11 and 18) show that, with 20 mol % of KO^{t}Bu as the base additive, *cis,anti*-**7′** and **8** (a 32:68 mixture of *cis,anti* and *cis,syn* isomers) exhibit some catalytic activity for the hydrogenation of PhCO$_2$CH$_2$Ph to PhCH$_2$OH, although the yield is very low (3−4%). Switching the solvent from THF to EtOH does not improve the hydrogenation reaction, only leading to transesterification of PhCO$_2$CH$_2$Ph to PhCO$_2$Et (entries 12, 14, and 19). Adding 20 mol % of NaOEt to *cis,anti*-**8** (or the *cis,anti* and *cis,syn* mixture) increases the yield of PhCH$_2$OH to 86% (entry 15 or 20); however, only a small fraction (12%) stems from the hydrogenation process.

To differentiate between the reactivity of *cis,anti*-**8** and *cis,syn*-**8**, catalytic hydrogenation of PhCHO was studied at a temperature (60 °C) where the geometric isomerization was insignificant. Under the conditions outlined in Scheme 10, the *cis,anti* isomer shows no catalytic activity at all. In contrast, the *cis,syn* isomer converts 45% of the PhCHO to PhCH$_2$OH,

Scheme 10. Distinct Catalytic Activity Displayed by the Two Isomers

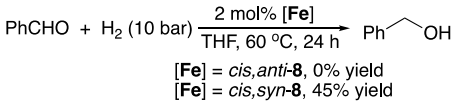

providing strong evidence that an active hydrogenation catalyst requires a *syn* configuration for the H−N−Fe−H unit.

For further mechanistic elucidation, stoichiometric reactions between the cationic hydrides and PhCHO were investigated at room temperature (Scheme 11). Over a period of 48 h, *cis,anti*-**8** failed to react with PhCHO, as did *cis,anti*-**7** containing the mixed counterions. The lack of reactivity could be due to thermodynamics, although the lack of H/D exchange between *cis,anti*-**8** and PhCDO suggests that the H$^-$ transfer step alone is kinetically unfavorable. Conversely, *cis,syn*-**8** reacted with PhCHO within hours, likely reversibly, to yield a complicated mixture (at least two benzyloxy-containing species on the basis of the ^{1}H NMR spectrum and at least three iron complexes on the basis of the ^{31}P{^{1}H} NMR spectrum). Full consumption of *cis,syn*-**8** took approximately 1 week, at which point the major benzyloxy-containing product was identified as PhCH$_2$OH (δ_H 4.57 ppm)[44] and the major iron complex displayed a phosphorus resonance at 80.8 ppm. Attempts to isolate the intermediates and products through crystallization were fruitless. We propose that PhCHO undergoes carbonyl reduction with *cis,syn*-**8** to form a transient alkoxide complex, which reacts slowly with CD$_3$CN to give [(^{iPr}PNP)Fe(NCCD$_3$)(CN^{t}Bu)$_2$]BPh$_4$ (Scheme 11). The kinetic barrier for H$^-$ transfer is lowered with *cis,syn*-**8**, presumably due to activation of the carbonyl group and stabilization of PhCH$_2$O$^-$ by the *syn* NH hydrogen.

https://doi.org/10.1021/acs.inorgchem.1c00328
Inorg. Chem. 2021, 60, 6521−6535

Scheme 11. Stoichiometric Reactions of *cis,anti*-8 and *cis,syn*-8 with Benzaldehyde

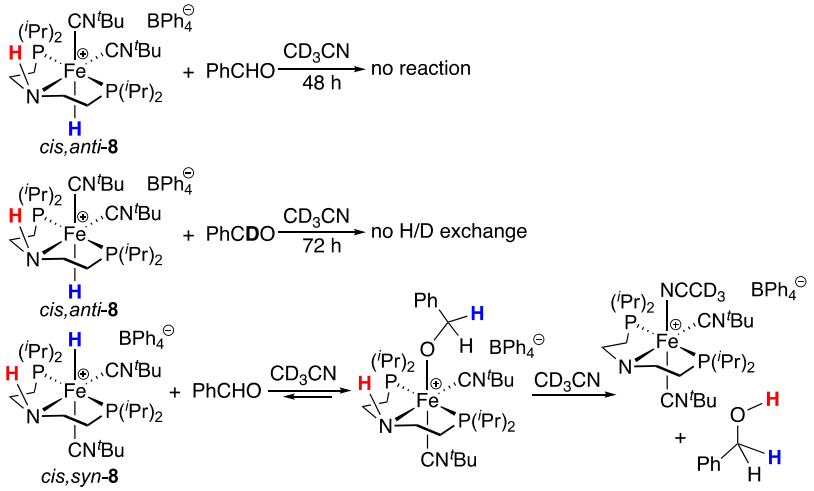

Scheme 12. Mechanistic Reasoning for the Reduction of PhCHO with the *cis,anti* and *cis,syn* Isomers[a]

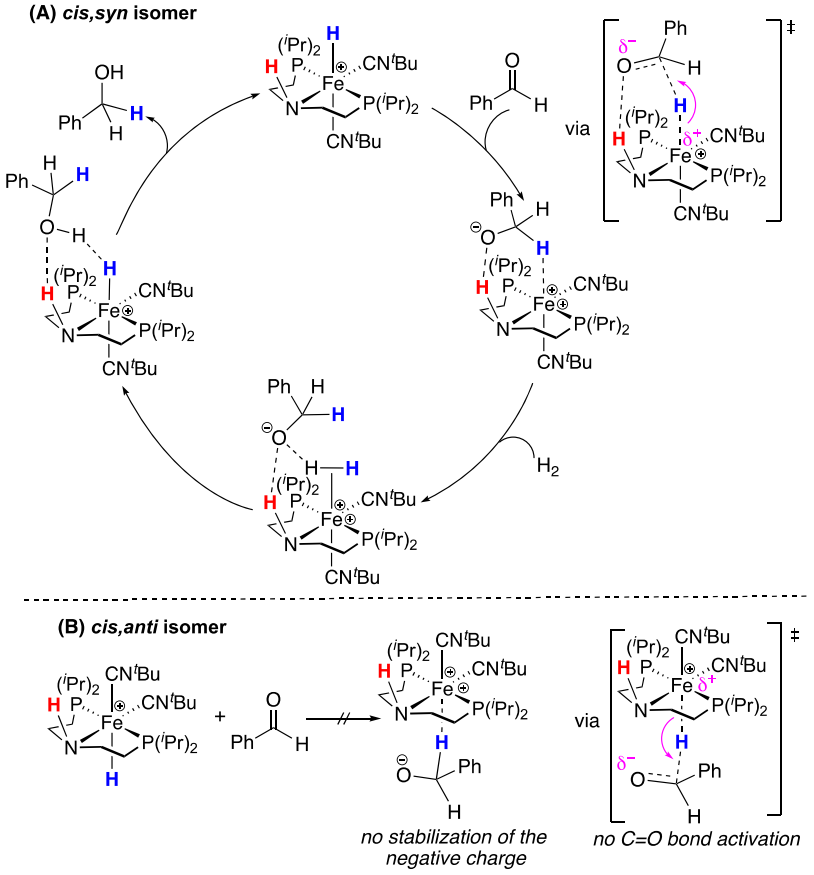

[a]The BPh_4 counterion is omitted for clarity.

CONCLUSIONS

In this work, we have synthesized and characterized a number of iron hydride complexes, each featuring a PNP pincer ligand and at least one isocyanide ligand. The neutral hydrido borohydride complexes $(^{R}PN^{H}P)FeH(CNR')(BH_4)$ catalyze the hydrogenation of $PhCO_2CH_2Ph$ to $PhCH_2OH$, though less efficiently than the carbonyl derivative $(^{iPr}PN^{H}P)FeH(CO)(BH_4)$. The cationic bis(isocyanide) hydride $[(^{iPr}PN^{H}P)FeH(CN^{t}Bu)_2]^+$ can be obtained as a *cis,anti* or *cis,syn* isomer or a mixture of the two, and the positive charge can be balanced with tetraphenylborate, bromide, or a mixture of bromide and borohydride. The relative stabilities of the *cis,anti* and *cis,syn* isomers depend on whether or not the counterion forms a hydrogen bond with the NH group. These cationic hydride complexes are virtually inactive catalysts for ester hydrogenation, likely due to reduced hydricity. However, *cis,syn*-$[(^{iPr}PN^{H}P)FeH(CN^{t}Bu)_2]BPh_4$ can catalyze the hydrogenation of PhCHO, whereas the *cis,anti* isomer cannot. This result is consistent with the current mechanistic understanding of C═O

https://doi.org/10.1021/acs.inorgchem.1c00328
Inorg. Chem. 2021, 60, 6521−6535

bond hydrogenation catalyzed by H−N−M−H type complexes. As illustrated in Scheme 12, the *cis,syn* isomer has the "right" NH configuration that can stabilize the ion-pair intermediate through hydrogen-bonding interactions, which in turn assist the subsequent dihydrogen activation. The NH group may also help activate the C═O bond during hydride transfer. The stabilization of the negative charge and the C═O bond activation are absent with the *cis,anti* isomer, which explains its inertness toward PhCHO in both stochiometric and catalytic reactions.

EXPERIMENTAL SECTION

General Considerations. All compounds described in this paper were prepared under an argon atmosphere using standard glovebox and Schlenk techniques. Benzene-d_6 and benzene were dried over sodium-benzophenone and distilled under an argon atmosphere. Acetonitrile-d_3 and methylene chloride-d_2 were purchased from Cambridge Isotope Laboratories, Inc., and used as received without further purification. Ethanol, chlorobenzene, and acetonitrile were dried over 4 Å molecular sieves and then deoxygenated by bubbling argon through them for 1 h. All other dry and oxygen-free solvents used for synthesis and workup (THF, diethyl ether, toluene, and pentane) were collected from an Innovative Technology solvent purification system. Benzaldehyde was freshly distilled prior to use. $HN(CH_2CH_2P^iPr_2)_2$ ($^{iPr}PN^HP$),[45] $HN(CH_2CH_2PCy_2)_2$ ($^{Cy}PN^HP$),[46] and ($^{iPr}PN^HP$)FeH(CNAr)(BH_4) (**1**, Ar = 2,6-dimethylphenyl)[9f] were prepared according to literature procedures. ^{1}H, $^{13}C\{^1H\}$, and $^{31}P\{^1H\}$ NMR spectra were recorded on a Bruker Avance 400 MHz NMR spectrometer. Chemical shift values in ^{1}H and $^{13}C\{^1H\}$ NMR spectra were referenced internally to the residual solvent resonances. $^{31}P\{^1H\}$ NMR spectra were referenced externally to 85% H_3PO_4 (0 ppm). Infrared spectra were recorded on a PerkinElmer Spectrum Two FT-IR spectrometer equipped with a smart orbit diamond attenuated total reflectance (ATR) accessory. Experimental details for the synthesis of **4** (*trans* and *cis,anti* mixture), *cis,anti*-**4**, **5** (*trans* and *cis,anti* mixture), *trans*-**5**, *cis,anti*-**5**, *cis,syn*-**5**, *cis,anti*-**7**, *cis,anti*-**7′**, and **8** (*cis,anti* and *cis,syn* mixture) are provided in the Supporting Information.

Synthesis of ($^{iPr}PN^HP$)FeH(CN^tBu)(BH_4) (2). Under an argon atmosphere, in an oven-dried Schlenk flask equipped with a stir bar were placed $^{iPr}PN^HP$ (305 mg, 1.0 mmol), $FeCl_2$ (127 mg, 1.0 mmol), and 70 mL of THF. The resulting mixture was refluxed for 2 h, giving a light yellow solution. The flask was then cooled to 0 °C in an ice−water bath, after which a solution of *tert*-butyl isocyanide (113 μL, 1.0 mmol) in 10 mL of THF was added dropwise. The green solution obtained was slowly warmed to room temperature and further stirred for 1 h. A solution of $NaBH_4$ (189 mg, 5.0 mmol) in 60 mL of EtOH was added, resulting in an intermediate color change from green to orange and eventually to yellow. After 16 h, the volatiles were removed under vacuum and the residue was treated with 60 mL of toluene. Filtration through a short pad of Celite followed by removal of the solvent under vacuum afforded the product as a bright yellow powder (210 mg, 46% yield). Orange-yellow crystals suitable for an X-ray crystallographic study were grown from toluene. ^{1}H NMR (400 MHz, C_6D_6, δ): 3.72−3.58 (m, N*H*, 1H), 2.97−2.77 (m, 2H), 2.63−2.44 (m, 2H), 2.26−2.10 (m, 2H), 1.82−1.70 (m, 2H), 1.69−1.56 (m, 6H for $PCH(CH_3)_2$ + 2H for C*H* or CH_2), 1.54−1.42 (m, 2H), 1.36−1.26 (m, $PCH(CH_3)_2$,6H), 1.25−1.16 (m, $PCH(CH_3)_2$,6H), 1.09−0.99 (m, $PCH(CH_3)_2$,6H), 1.06 (s, $CNC(CH_3)_3$, 9H), −3.06 (br, BH_4, 4H), −21.80 (t, J_{H-P} = 52.7 Hz, Fe*H*, 1H). $^{13}C\{^1H\}$ (101 MHz, C_6D_6, δ): 184.0−183.3 (m, *C*$NC(CH_3)_3$), 55.2 (s, $CNC(CH_3)_3$), 53.8 (t, J_{P-C} = 5.7 Hz, NCH_2), 31.1 (s, $CNC(CH_3)_3$), 29.5 (t, J_{P-C} = 7.6 Hz), 29.2 (t, J_{P-C} = 6.3 Hz), 26.0 (td, J_{P-C} = 11.6 Hz, J = 2.7 Hz), 21.4 (s, $PCH(CH_3)_2$), 20.9 (t, J_{P-C} = 2.5 Hz, $PCH(CH_3)_2$), 19.3 (s, $PCH(CH_3)_2$), 18.9 (s, $PCH(CH_3)_2$). $^{31}P\{^1H\}$ NMR (162 MHz, C_6D_6, δ): 99.2 (s). Selected ATR-IR data (solid, cm^{-1}): 3206 (ν_{N-H}), 2339 ($\nu_{B-H,terminal}$), 2327 ($\nu_{B-H,terminal}$), 2296 ($\nu_{B-H,terminal}$), 2000 ($\nu_{C\equiv N}$), 1782 (ν_{Fe-H}); $\nu_{B-H,bridging}$ could not be definitively assigned. Anal. Calcd for $C_{21}H_{51}N_2BP_2Fe$: C, 54.80; H, 11.17; N, 6.09. Found: C, 54.53; H, 11.32; N, 5.93.

Synthesis of ($^{Cy}PN^HP$)FeH(CNAr)(BH_4) (3; Ar = 2,6-Dimethylphenyl). Following the same procedure used for **2**, hydride **3** was isolated as a bright yellow powder in 45% yield (300 mg from a 1.0 mmol scale reaction). Yellow crystals suitable for an X-ray crystallographic analysis were grown from toluene. ^{1}H NMR (400 MHz, C_6D_6, δ): 6.86 (d, J_{H-H} = 7.2 Hz, Ar*H*, 2H), 6.74 (t, J_{H-H} = 7.2 Hz, Ar*H*, 1H), 3.96−3.84 (m, N*H*, 1H), 2.82−2.71 (m, 2H), 2.70−2.48 (m, 4H), 2.55 (s, ArCH_3, 6H), 2.05−1.05 (m, 44H from Cy*H* + 2H from the pincer backbone), −3.06 (br, BH_4, 4H), −21.23 (t, J_{H-P} = 52.8 Hz, Fe*H*, 1H). $^{13}C\{^1H\}$ NMR (101 MHz, C_6D_6, δ): 199.1−198.4 (m, *C*NAr), 133.4 (s, Ar*C*), 133.3 (s, Ar*C*), 128.2 (s, Ar*C*), 123.9 (s, Ar*C*), 54.0 (t, J_{P-C} = 5.8 Hz, NCH_2), 40.2 (t, J_{P-C} = 7.9 Hz), 37.1 (t, J_{P-C} = 12.8 Hz), 31.1 (s, Cy*C*), 30.8 (s, Cy*C*), 29.4 (s, Cy*C*), 28.5 (s, Cy*C*), 28.2 (t, J_{P-C} = 6.1 Hz), 27.9 (t, J_{P-C} = 3.7 Hz), 27.8 (t, J_{P-C} = 6.7 Hz), 27.5 (t, J_{P-C} = 4.6 Hz), 27.3 (t, J_{P-C} = 5.8 Hz), 27.03 (s, Cy*C*), 26.95 (s, Cy*C*), 19.0 (s, CH_3). $^{31}P\{^1H\}$ NMR (162 MHz, C_6D_6, δ): 90.2 (s). Selected ATR-IR data (solid, cm^{-1}): 3201 (ν_{N-H}), 2341 ($\nu_{B-H,terminal}$), 2325 ($\nu_{B-H,terminal}$), 2032 ($\nu_{B-H,bridging}$), 1973 ($\nu_{C\equiv N}$), 1835 (ν_{Fe-H}). Elemental analysis data were unsatisfactory despite repeated trials; however, the data match the values calculated for an oxidized product. Anal. Calcd for $C_{37}H_{67}N_2BP_2Fe$ (**3**): C, 66.47; H, 10.10; N, 4.19. Calcd for $C_{37}H_{67}N_2O_2BP_2Fe$ (**3** + O_2): C, 63.44; H, 9.64; N, 4.00. Found: C, 63.41; H, 9.38; N, 3.82.

Synthesis of *cis,anti*-[($^{iPr}PN^HP$)FeH($CN^tBu)_2$]BPh_4 (*cis,anti*-8). In a glovebox, in a 100 mL oven-dried Schlenk flask equipped with a stir bar were placed *cis,anti*-[($^{iPr}PN^HP$)FeH($CN^tBu)_2$]X (*cis,anti*-**7**, X = 67% Br and 33% BH_4, 232 mg, 0.40 mmol) and $NaBPh_4$ (220 mg, 0.64 mmol). The flask was then connected to a Schlenk line, after which 30 mL of ethanol was added. The resulting suspension was stirred at room temperature for 1 h before a cannula filtration was performed. The collected solid was dried under vacuum to afford the desired product as a white powder (178 mg, 53% yield). Colorless crystals suitable for X-ray crystallography were grown from CH_3CN−EtOH. ^{1}H NMR (400 MHz, CD_3CN, δ): 7.31−7.24 (m, Ar*H*, 8H), 6.99 (t, J_{H-H} = 7.2 Hz, Ar*H*, 8H), 6.84 (t, J_{H-H} = 7.2 Hz, Ar*H*, 4H), 3.08−2.96 (m, N*H*, 1H), 2.87−2.72 (m, 2H), 2.46−2.36 (m, 2H), 2.34−2.25 (m, 2H), 2.20−2.09 (m, 2H), 1.87−1.71 (m, 2H), 1.52−1.39 (m, 6H for $PCH(CH_3)_2$ + 2H for C*H* or CH_2), 1.47 (s, $CNC(CH_3)_3$, 9H), 1.38−1.30 (m, $PCH(CH_3)_2$, 6H), 1.27−1.17 (m, $PCH(CH_3)_2$, 12H), 1.22 (s, $CNC(CH_3)_3$, 9H), −10.28 (t, J_{P-H} = 51.6 Hz, Fe*H*, 1H). $^{13}C\{^1H\}$ NMR (101 MHz, CD_3CN, δ): 164.8 (q, J_{C-B} = 49.5 Hz, Ar*C*), 136.7 (q, J_{C-B} = 1.2 Hz, Ar*C*), 126.6 (q, J_{C-B} = 2.7 Hz, Ar*C*), 122.7 (s, Ar*C*), 57.12 (s, $CNC(CH_3)_3$), 57.09 (s, $CNC(CH_3)_3$), 54.6 (t, J_{P-C} = 4.6 Hz, NCH_2), 31.9 (t, J_{P-C} = 9.1 Hz), 31.2 (s, $CNC(CH_3)_3$), 30.9 (s, $CNC(CH_3)_3$), 29.4 (t, J_{P-C} = 9.1 Hz), 26.4 (t, J_{P-C} = 13.6 Hz), 21.1 (t, J_{P-C} = 1.8 Hz, $PCH(CH_3)_2$), 20.7 (s, $PCH(CH_3)_2$), 19.13 (s, $PCH(CH_3)_2$), 19.08 (s, $PCH(CH_3)_2$); the isocyanide N*C* resonances were not located. $^{31}P\{^1H\}$ NMR (162 MHz, CD_3CN, δ): 100.7 (s). Selected ATR-IR data (solid, cm^{-1}): 2103 ($\nu_{C\equiv N}$), 2037 ($\nu_{C\equiv N}$), 1791 (ν_{Fe-H}). Anal. Calcd for $C_{50}H_{76}N_3BP_2Fe$: C, 70.84; H, 9.04; N, 4.96. Found: C, 70.54; H, 9.06; N, 4.90.

***cis,syn*-[($^{iPr}PN^HP$)FeH($CN^tBu)_2$]BPh_4 (*cis,syn*-8) Obtained via Recrystallization.** In a glovebox, a 32:68 mixture of *cis,anti*-**8** and *cis,syn*-**8** (50 mg, 0.059 mmol) was dissolved in 1 mL of THF in a scintillation vial. The resulting light yellow solution was carefully layered with 1 mL of ethanol. Storing the vial in a−30 °C freezer for 3 days resulted in the formation of colorless crystals, which were collected by decanting off the supernatant and then dried under vacuum. The isolated product was identified as *cis,syn*-**8** with 98% purity (25 mg, 50% recovery yield). Colorless crystals suitable for an X-ray crystallographic study were grown from THF−EtOH. ^{1}H NMR (400 MHz, CD_3CN, δ): 7.33−7.25 (m, Ar*H*, 8H), 7.01 (t, J_{H-H} = 7.2 Hz, Ar*H*, 8H), 6.85 (t, J_{H-H} = 7.2 Hz, Ar*H*, 4H), 2.88−2.70 (m, 1H for N*H* + 2H for C*H* or CH_2), 2.37−2.24 (m, 4H), 2.10−2.00 (m, 2H), 1.99−1.87 (m, 2H), 1.54−1.43 (m, 6H for $PCH(CH_3)_2$ + 2H for C*H* or CH_2), 1.47 (s, $CNC(CH_3)_3$, 9H), 1.42−1.35 (m, $PCH(CH_3)_2$, 6H), 1.28−1.20 (m, $PCH(CH_3)_2$, 12H), 1.22 (s, $CNC(CH_3)_3$, 9H), −9.75 (t, J_{P-H} = 53.2 Hz, Fe*H*, 1H). $^{13}C\{^1H\}$ NMR (101 MHz, CD_3CN, δ): 164.8 (q, J_{C-B} = 49.5 Hz, Ar*C*), 136.7 (q, J_{C-B} = 1.2 Hz, Ar*C*), 126.6 (q, J_{C-B} = 2.8 Hz, Ar*C*), 122.7 (s, Ar*C*), 57.3 (s, $CNC(CH_3)_3$), 57.0 (s, $CNC(CH_3)_3$),

https://doi.org/10.1021/acs.inorgchem.1c00328
Inorg. Chem. 2021, 60, 6521−6535

52.8 (t, J_{P-C} = 5.2 Hz, NCH_2), 31.1 (s, $CNC(CH_3)_3$), 30.9 (s, $CNC(CH_3)_3$), 29.9 (t, J_{P-C} = 8.0 Hz), 26.7 (t, J_{P-C} = 13.6 Hz), 26.6 (t, J_{P-C} = 8.6 Hz), 20.7 (s, $PCH(CH_3)_2$), 20.6 (s, $PCH(CH_3)_2$), 19.5 (s, $PCH(CH_3)_2$), 18.9 (s, $PCH(CH_3)_2$); the isocyanide NC resonances were not located. $^{31}P\{^1H\}$ NMR (162 MHz, CD_3CN, δ): 103.4 (s). Selected ATR-IR data (solid, cm^{-1}): 3244 (ν_{N-H}), 2098 ($\nu_{C\equiv N}$), 2032 ($\nu_{C\equiv N}$), 1814 (ν_{Fe-H}). Anal. Calcd for $C_{50}H_{76}N_3BP_2Fe$: C, 70.84; H, 9.04; N, 4.96. Found: C, 70.59; H, 9.24; N, 4.87.

Procedure for Iron-Catalyzed Hydrogenation of Benzyl Benzoate or Benzaldehyde. Under an argon atmosphere, benzyl benzoate or benzaldehyde (1.0 mmol), an iron hydride complex (0.020 mmol, 2 mol % catalyst loading), base additive (if applicable, 0.20 mmol, 20 mol %), and bibenzyl (91 mg, 0.50 mmol, an internal standard) were mixed with 0.5 mL of THF or EtOH in a glass tube. The tube was then placed in a high-pressure reactor, which was flushed with 5 bar of H_2 three times before being placed under 10 bar of H_2 pressure. The reaction was carried out at 60 °C (for PhCHO) or 110 °C (for $PhCO_2CH_2Ph$) with stirring for an appropriate time. When the reaction was stopped, the reactor was cooled to room temperature and the residual dihydrogen was carefully released. The reaction solution was passed through a pad of silica gel, which was eluted with ethyl acetate. The volatiles were removed under vacuum, and the residue was analyzed by ^1H NMR spectroscopy to calculate the conversion and yield.

Procedure for the Stoichiometric Reaction between an Iron Hydride and Benzaldehyde. Under an argon atmosphere, in a J. Young NMR tube were placed an iron hydride complex (0.024 mmol), benzaldehyde (0.024 mmol), and ~0.5 mL of a deuterated solvent (C_6D_6 for the reaction with *cis,anti*-**7** and CD_3CN for the reaction with *cis,anti*-**8** or *cis,syn*-**8**). The progress of the reaction was monitored by ^1H and $^{31}P\{^1H\}$ NMR spectroscopy.

X-ray Structure Determinations. Crystal data collection and refinement parameters are provided in the Supporting Information. Single crystals of **1** (orange−yellow) were grown from THF−pentane. Details on how single crystals were obtained for the other iron complexes are described in the corresponding synthesis and characterization subsections. Intensity data for **1**, **2**, *cis,anti*-**5**·2THF,*cis,syn*-**5**, *cis,anti*-**7′**·1/2H_2O, and *cis,syn*-**8** were collected at 150 K on a Bruker D8 Venture Photon-II diffractometer with Mo Kα radiation, λ = 0.71073 Å. Intensity data for *trans*-**5**·MeCN were collected at 150 K on a standard Bruker APEX-II CCD diffractometer with Mo Kα radiation. Intensity data for *cis*-**6**·3/4C_2H_5NO·3/4MeCN were collected at 150 K on a Bruker DUO APEX-II CCD diffractometer at the University of Notre Dame using Mo Kα radiation. Intensity data for the remaining compounds were collected at 150 K on a Bruker PHOTON-II (**3** and *cis,anti*-**4**·1/2C_7H_8) or PHOTON100 CMOS detector (*cis,anti*-**8**) at Beamline 11.3.1 at the Advanced Light Source (Lawrence Berkeley National Laboratory) using synchrotron radiation tuned to λ = 0.7749 Å. The data frames were processed using the program SAINT. The data were corrected for decay, Lorentz, and polarization effects as well as absorption and beam corrections based on the multiscan technique in SADABS. The structures were solved by a combination of direct methods and the difference Fourier technique as implemented in the SHELX suite of programs and refined by full-matrix least squares on F^2. Non-hydrogen atoms were refined with anisotropic displacement parameters with the exception of the minor component of the disordered atoms. The Fe-, N-, B-, and O-bound hydrogen atoms in all structures except *cis*-**6**·3/4C_2H_5NO·3/4MeCN were located directly from the difference map, and the coordinates were refined. The bridging H−B in **3** was restrained to the CSD average distance for an Fe−H−BH_3 type linkage. The remaining hydrogen atoms were calculated and treated with a riding model. **1** was refined as a two-component twin (twin law: −1,0,0 0,−1,0 0.069,0,1; 24% twin; CELL_NOW). One cyclohexyl ring of **3**, one *tert*-butyl group, and the cocrystallized half toluene molecule of *cis,anti*-**4**·1/2C_7H_8, one cocrystallized THF molecule of *cis,anti*-**5**·2THF, one *tert*-butyl group of *cis,syn*-**5**, and one isopropyl group along with the pincer backbone of *cis*-**6**·3/4C_2H_5NO·3/4MeCN were disordered and were refined with a two-component model. In *cis*-**6**·3/4C_2H_5NO·3/4MeCN, the (*Z*)-methylimidoformic acid (or the enol form of *N*-methylformamide) and acetonitrile of crystallization were modeled as partially occupied molecules (occupancies were initially refined to approximately 75%; they were fixed at 0.75 in the final refinement cycles). **1** crystallizes as two independent molecules in the lattice. *cis,anti*-**7′**·1/2H_2O crystallizes as two independent molecules in the lattice; in each molecule, one *tert*-butyl group was disordered and was refined with a two-component model. Crystal structures mentioned in this paper have been deposited at the Cambridge Crystallographic Data Centre (CCDC) and allocated the deposition numbers CCDC 2058976−2058986.

■ ASSOCIATED CONTENT

Supporting Information

The Supporting Information is available free of charge at https://pubs.acs.org/doi/10.1021/acs.inorgchem.1c00328.

Additional experimental details, NMR and IR spectra of the iron pincer complexes, and X-ray crystallographic information (PDF)

Accession Codes

CCDC 2058976−2058986 contain the supplementary crystallographic data for this paper. These data can be obtained free of charge via www.ccdc.cam.ac.uk/data_request/cif, or by emailing data_request@ccdc.cam.ac.uk, or by contacting The Cambridge Crystallographic Data Centre, 12 Union Road, Cambridge CB2 1EZ, UK; fax: +44 1223 336033.

■ AUTHOR INFORMATION

Corresponding Author

Hairong Guan − *Department of Chemistry, University of Cincinnati, Cincinnati, Ohio 45221-0172, United States;* orcid.org/0000-0002-4858-3159; Email: hairong.guan@uc.edu

Authors

Huiguang Dai − *Department of Chemistry, University of Cincinnati, Cincinnati, Ohio 45221-0172, United States*

Weishi Li − *Department of Chemistry, University of Cincinnati, Cincinnati, Ohio 45221-0172, United States*

Jeanette A. Krause − *Department of Chemistry, University of Cincinnati, Cincinnati, Ohio 45221-0172, United States*

Complete contact information is available at: https://pubs.acs.org/10.1021/acs.inorgchem.1c00328

Notes

The authors declare no competing financial interest.

■ ACKNOWLEDGMENTS

We thank the NSF Chemical Catalysis Program (CHE-1464734 and CHE-1800151) and the University of Cincinnati (Doctoral Enhancement Research Fellowship to H.D.) for support of this research, Professor David F. Watson (University at Buffalo) for the suggestion of using isocyanide ligands, Professor Nilay Hazari (Yale University) for helpful discussions, and Professor Allen G. Oliver (University of Notre Dame) for data collection on a Bruker DUO APEX-II CCD diffractometer. Crystallographic data were also collected on a Bruker APEX-II CCD diffractometer (funded by NSF-MRI grant CHE-0215950), on a Bruker D8 Venture diffractometer (funded by NSF-MRI grant CHE-1625737), or through the SCrALS (Service Crystallography at Advanced Light Source) Program at Beamline 11.3.1 at the Advanced Light Source (ALS), Lawrence Berkeley National Laboratory (funded by the U.S. Department of Energy, Office of Basic Energy Sciences, under contract No. DE-AC02-

https://doi.org/10.1021/acs.inorgchem.1c00328
Inorg. Chem. 2021, 60, 6521−6535

05CH11231). We wish to dedicate this paper to the memory of Professor William B. Connick, a brilliant scientist, an inspirational teacher, and a wonderful friend, whose suggestions were instrumental to the completion of this work.

REFERENCES

(1) (a) Morris, R. H. Exploiting Metal-Ligand Bifunctional Reactions in the Design of Iron Asymmetric Hydrogenation Catalysts. *Acc. Chem. Res.* **2015**, *48*, 1494−1502. (b) Zell, T.; Milstein, D. Hydrogenation and Dehydrogenation Iron Pincer Catalysts Capable of Metal-Ligand Cooperation by Aromatization/Dearomatization. *Acc. Chem. Res.* **2015**, *48*, 1979−1994. (c) Chakraborty, S.; Bhattacharya, P.; Dai, H.; Guan, H. Nickel and Iron Pincer Complexes as Catalysts for the Reduction of Carbonyl Compounds. *Acc. Chem. Res.* **2015**, *48*, 1995−2003. (d) Werkmeister, S.; Neumann, J.; Junge, K.; Beller, M. Pincer-Type Complexes for Catalytic (De)Hydrogenation and Transfer (De)-Hydrogenation Reactions: Recent Progress. *Chem. - Eur. J.* **2015**, *21*, 12226−12250. (e) Bernskoetter, W. H.; Hazari, N. Reversible Hydrogenation of Carbon Dioxide to Formic Acid and Methanol: Lewis Acid Enhancement of Base Metal Catalysts. *Acc. Chem. Res.* **2017**, *50*, 1049−1058. (f) Filonenko, G. A.; van Putten, R.; Hensen, E. J. M.; Pidko, E. A. Catalytic (De)Hydrogenation Promoted by Non-precious Metals - Co, Fe and Mn: Recent Advances in an Emerging Field. *Chem. Soc. Rev.* **2018**, *47*, 1459−1483. (g) Gorgas, N.; Kirchner, K. Isoelectronic Manganese and Iron Hydrogenation/Dehydrogenation Catalysts: Similarities and Divergences. *Acc. Chem. Res.* **2018**, *51*, 1558−1569. (h) Seo, C. S. G.; Morris, R. H. Catalytic Homogeneous Asymmetric Hydrogenation: Successes and Opportunities. *Organometallics* **2019**, *38*, 47−65. (i) Wei, D.; Darcel, C. Iron Catalysis in Reduction and Hydrometalation Reactions. *Chem. Rev.* **2019**, *119*, 2550−2610. (j) Alig, L.; Fritz, M.; Schneider, S. First-Row Transition Metal (De)Hydrogenation Catalysis Based On Functional Pincer Ligands. *Chem. Rev.* **2019**, *119*, 2681−2751.

(2) (a) Knölker, H.-J.; Baum, E.; Goesmann, H.; Klauss, R. Demetalation of Tricarbonyl(cyclopentadienone)iron Complexes Initiated by a Ligand Exchange Reaction with NaOH - X-ray Analysis of a Complex with Nearly Square-Planar Coordinated Sodium. *Angew. Chem., Int. Ed.* **1999**, *38*, 2064−2066. (b) Chakraborty, A.; Guan, H. Iron, dicarbonylhydro[(1,2,3,3a,7a-η)-4,5,6,7-tetrahydro-2-hydroxy-1,3-bis(trimethylsilyl)-1*H*-inden-1-yl]-. *e-Encyclopedia of Reagents for Organic Synthesis*; Wiley: 2014.

(3) (a) Casey, C. P.; Guan, H. An Efficient and Chemoselective Iron Catalyst for the Hydrogenation of Ketones. *J. Am. Chem. Soc.* **2007**, *129*, 5816−5817. (b) Casey, C. P.; Guan, H. Cyclopentadienone Iron Alcohol Complexes: Synthesis, Reactivity, and Implications for the Mechanism of Iron-Catalyzed Hydrogenation of Aldehydes. *J. Am. Chem. Soc.* **2009**, *131*, 2499−2507.

(4) (a) Sui-Seng, C.; Freutel, F.; Lough, A. J.; Morris, R. H. Highly Efficient Catalyst Systems Using Iron Complexes with a Tetradentate PNNP Ligand for the Asymmetric Hydrogenation of Polar Bonds. *Angew. Chem., Int. Ed.* **2008**, *47*, 940−943. (b) Sui-Seng, C.; Haque, F. N.; Hadzovic, A.; Pütz, A.-M.; Reuss, V.; Meyer, N.; Lough, A. J.; Zimmer-De Iuliis, M.; Morris, R. H. Synthesis and Characterization of Iron(II) Complexes with Tetradentate Diiminodiphosphine or Diaminodiphosphine Ligands as Precatalysts for the Hydrogenation of Acetophenone. *Inorg. Chem.* **2009**, *48*, 735−743.

(5) Pincer-type catalysts: (a) Langer, R.; Leitus, G.; Ben-David, Y.; Milstein, D. Efficient Hydrogenation of Ketones Catalyzed by an Iron Pincer Complex. *Angew. Chem., Int. Ed.* **2011**, *50*, 2120−2124. (b) Langer, R.; Iron, M. A.; Konstantinovski, L.; Diskin-Posner, Y.; Leitus, G.; Ben-David, Y.; Milstein, D. Iron Borohydride Pincer Complexes for the Efficient Hydrogenation of Ketones Under Mild, Base-Free Conditions: Synthesis and Mechanistic Insight. *Chem. - Eur. J.* **2012**, *18*, 7196−7209. (c) Chakraborty, S.; Lagaditis, P. O.; Förster, M.; Bielinski, E. A.; Hazari, N.; Holthausen, M. C.; Jones, W. D.; Schneider, S. Well-Defined Iron Catalysts for the Acceptorless Reversible Dehydrogenation-Hydrogenation of Alcohols and Ketones. *ACS Catal.* **2014**, *4*, 3994−4003. (d) Gorgas, N.; Stöger, B.; Veiros, L. F.; Pittenauer, E.; Allmaier, G.; Kirchner, K. Efficient Hydrogenation of Ketones and Aldehydes Catalyzed by Well-Defined Iron(II) PNP Pincer Complexes: Evidence for an Insertion Mechanism. *Organometallics* **2014**, *33*, 6905−6914. (e) Mazza, S.; Scopelliti, R.; Hu, X. Chemoselective Hydrogenation and Transfer Hydrogenation of Aldehydes Catalyzed by Iron(II) PONOP Pincer Complexes. *Organometallics* **2015**, *34*, 1538−1545. (f) Zell, T.; Ben-David, Y.; Milstein, D. Highly Efficient, General Hydrogenation of Aldehydes Catalyzed by PNP Iron Pincer Complexes. *Catal. Sci. Technol.* **2015**, *5*, 822−826. (g) Gorgas, N.; Stöger, B.; Veiros, L. F.; Kirchner, K. Highly Efficient and Selective Hydrogenation of Aldehydes: A Well-Defined Fe(II) Catalyst Exhibits Noble-Metal Activity. *ACS Catal.* **2016**, *6*, 2664−2672. (h) Butschke, B.; Feller, M.; Diskin-Posner, Y.; Milstein, D. Ketone Hydrogenation Catalyzed by a New Iron(II)-PNN Complex. *Catal. Sci. Technol.* **2016**, *6*, 4428−4437. (i) Brünig, J.; Csendes, Z.; Weber, S.; Gorgas, N.; Bittner, R. W.; Limbeck, A.; Bica, K.; Hoffmann, H.; Kirchner, K. Chemoselective Supported Ionic-Liquid-Phase (SILP) Aldehyde Hydrogenation Catalyzed by an Fe(II) PNP Pincer Complex. *ACS Catal.* **2018**, *8*, 1048−1051.

(6) Nonpincer-type catalysts: (a) Fleischer, S.; Zhou, S.; Junge, K.; Beller, M. General and Highly Efficient Iron-Catalyzed Hydrogenation of Aldehydes, Ketones, and α,β-Unsaturated Aldehydes. *Angew. Chem., Int. Ed.* **2013**, *52*, 5120−5124. (b) Wienhöfer, G.; Westerhaus, F. A.; Junge, K.; Ludwig, R.; Beller, M. A Molecularly Defined Iron-Catalyst for the Selective Hydrogenation of α,β-Unsaturated Aldehydes. *Chem. - Eur. J.* **2013**, *19*, 7701−7707. (c) Lu, L.-Q.; Li, Y.; Junge, K.; Beller, M. Iron-Catalyzed Hydrogenation for the In Situ Regeneration of an NAD(P)H Model: Biomimetic Reduction of α-Keto-/α-Iminoesters. *Angew. Chem., Int. Ed.* **2013**, *52*, 8382−8386. (d) Mérel, D. S.; Elie, M.; Lohier, J.-F.; Gaillard, S.; Renaud, J.-L. Bifunctional Iron Complexes: Efficient Catalysts for C=O and C=N Reduction in Water. *ChemCatChem* **2013**, *5*, 2939−2945. (e) Vailati Facchini, S.; Neudörfl, J.-M.; Pignataro, L.; Cettolin, M.; Gennari, C.; Berkessel, A.; Piarulli, U. Synthesis of [Bis(hexamethylene)cyclopentadienone]-iron Tricarbonyl and Its Application to the Catalytic Reduction of C=O Bonds. *ChemCatChem* **2017**, *9*, 1461−1468.

(7) Pincer-type catalysts: (a) Lagaditis, P. O.; Sues, P. E.; Sonnenberg, J. F.; Wan, K. Y.; Lough, A. J.; Morris, R. H. Iron(II) Complexes Containing Unsymmetrical P-N-P' Pincer Ligands for the Catalytic Asymmetric Hydrogenation of Ketones and Imines. *J. Am. Chem. Soc.* **2014**, *136*, 1367−1380. (b) Sonnenberg, J. F.; Lagaditis, P. O.; Lough, A. J.; Morris, R. H. Synthesis of Iron P-N-P' and P-NH-P' Asymmetric Hydrogenation Catalysts. *Organometallics* **2014**, *33*, 6452−6465. (c) Zirakzadeh, A.; Kirchner, K.; Roller, A.; Stöger, B.; Widhalm, M.; Morris, R. H. Iron(II) Complexes Containing Chiral Unsymmetrical PNP′ Pincer Ligands: Synthesis and Application in Asymmetric Hydrogenations. *Organometallics* **2016**, *35*, 3781−3787. (d) Sonnenberg, J. F.; Wan, K. Y.; Sues, P. E.; Morris, R. H. Ketone Asymmetric Hydrogenation Catalyzed by P-NH-P' Pincer Iron Catalysts: An Experimental and Computational Study. *ACS Catal.* **2017**, *7*, 316−326. (e) Smith, S. A. M.; Lagaditis, P. O.; Lüpke, A.; Lough, A. J.; Morris, R. H. Unsymmetrical Iron P-NH-P′ Catalysts for the Asymmetric Pressure Hydrogenation of Aryl Ketones. *Chem. - Eur. J.* **2017**, *23*, 7212−7216. (f) Huber, R.; Passera, A.; Mezzetti, A. Iron(II)-Catalyzed Hydrogenation of Acetophenone with a Chiral, Pyridine-Based PNP Pincer Ligand: Support for an Outer-Sphere Mechanism. *Organometallics* **2018**, *37*, 396−405. (g) Huber, R.; Passera, A.; Gubler, E.; Mezzetti, A. P-Stereogenic PN(H)P Iron(II) Catalysts for the Asymmetric Hydrogenation of Ketones: The Importance of Non-Covalent Interactions in Rational Ligand Design by Computation. *Adv. Synth. Catal.* **2018**, *360*, 2900−2913. (h) Garbe, M.; Wei, Z.; Tannert, B.; Spannenberg, A.; Jiao, H.; Bachmann, S.; Scalone, M.; Junge, K.; Beller, M. Enantioselective Hydrogenation of Ketones Using Different Metal Complexes with a Chiral PNP Pincer Ligand. *Adv. Synth. Catal.* **2019**, *361*, 1913−1920.

(8) Nonpincer-type catalysts: (a) Berkessel, A.; Reichau, S.; von der Höh, A.; Leconte, N.; Neudörfl, J.-M. Light-Induced Enantioselective Hydrogenation Using Chiral Derivatives of Casey's Iron-Cyclopentadienone Catalyst. *Organometallics* **2011**, *30*, 3880−3887.

https://doi.org/10.1021/acs.inorgchem.1c00328
Inorg. Chem. 2021, 60, 6521−6535

(b) Zuo, W.; Tauer, S.; Prokopchuk, D. E.; Morris, R. H. Iron Catalysts Containing Amine(imine)diphosphine P-NH-N-P Ligands Catalyze both the Asymmetric Hydrogenation and Asymmetric Transfer Hydrogenation of Ketones. *Organometallics* **2014**, *33*, 5791−5801. (c) Li, Y.; Yu, S.; Wu, X.; Xiao, J.; Shen, W.; Dong, Z.; Gao, J. Iron Catalyzed Asymmetric Hydrogenation of Ketones. *J. Am. Chem. Soc.* **2014**, *136*, 4031−4039. (d) Gajewski, P.; Renom-Carrasco, M.; Vailati Facchini, S.; Pignataro, L.; Lefort, L.; de Vries, J. G.; Ferraccioli, R.; Forni, A.; Piarulli, U.; Gennari, C. Chiral (Cyclopentadienone)iron Complexes for the Catalytic Asymmetric Hydrogenation of Ketones. *Eur. J. Org. Chem.* **2015**, *2015*, 1887−1893. (e) Gajewski, P.; Renom-Carrasco, M.; Vailati Facchini, S.; Pignataro, L.; Lefort, L.; de Vries, J. G.; Ferraccioli, R.; Piarulli, U.; Gennari, C. Synthesis of (*R*)-BINOL-Derived (Cyclopentadienone)iron Complexes and Their Application in the Catalytic Asymmetric Hydrogenation of Ketones. *Eur. J. Org. Chem.* **2015**, *2015*, 5526−5536. (f) Hodgkinson, R.; Del Grosso, A.; Clarkson, G.; Wills, M. Iron Cyclopentadienone Complexes Derived from C_2-Symmetric Bis-Propargylic Alcohols; Preparation and Applications to Catalysis. *Dalton Trans.* **2016**, *45*, 3992−4005. (g) Del Grosso, A.; Chamberlain, A. E.; Clarkson, G. J.; Wills, M. Synthesis and Applications to Catalysis of Novel Cyclopentadienone Iron Tricarbonyl Complexes. *Dalton Trans.* **2018**, *47*, 1451−1470. (h) Bai, X.; Cettolin, M.; Mazzoccanti, G.; Pierini, M.; Piarulli, U.; Colombo, V.; Dal Corso, A.; Pignataro, L.; Gennari, C. Chiral (Cyclopentadienone)iron Complexes with a Stereogenic Plane as Pre-Catalysts for the Asymmetric Hydrogenation of Polar Double Bonds. *Tetrahedron* **2019**, *75*, 1415−1424.

(9) Pincer-type catalysts: (a) Langer, R.; Diskin-Posner, Y.; Leitus, G.; Shimon, L. J. W.; Ben-David, Y.; Milstein, D. Low-Pressure Hydrogenation of Carbon Dioxide Catalyzed by an Iron Pincer Complex Exhibiting Noble Metal Activity. *Angew. Chem., Int. Ed.* **2011**, *50*, 9948−9952. (b) Bielinski, E. A.; Lagaditis, P. O.; Zhang, Y.; Mercado, B. Q.; Würtele, C.; Bernskoetter, W. H.; Hazari, N.; Schneider, S. Lewis Acid-Assisted Formic Acid Dehydrogenation Using a Pincer-Supported Iron Catalyst. *J. Am. Chem. Soc.* **2014**, *136*, 10234−10237. (c) Zhang, Y.; MacIntosh, A. D.; Wong, J. L.; Bielinski, E. A.; Williard, P. G.; Mercado, B. Q.; Hazari, N.; Bernskoetter, W. H. Iron Catalyzed CO_2 Hydrogenation to Formate Enhanced by Lewis Acid Co-Catalysts. *Chem. Sci.* **2015**, *6*, 4291−4299. (d) Rivada-Wheelaghan, O.; Dauth, A.; Leitus, G.; Diskin-Posner, Y.; Milstein, D. Synthesis and Reactivity of Iron Complexes with a New Pyrazine-Based Pincer Ligand, and Application in Catalytic Low-Pressure Hydrogenation of Carbon Dioxide. *Inorg. Chem.* **2015**, *54*, 4526−4538. (e) Bertini, F.; Gorgas, N.; Stöger, B.; Peruzzini, M.; Veiros, L. F.; Kirchner, K.; Gonsalvi, L. Efficient and Mild Carbon Dioxide Hydrogenation to Formate Catalyzed by Fe(II) Hydrido Carbonyl Complexes Bearing 2,6-(Diaminopyridyl)diphosphine Pincer Ligands. *ACS Catal.* **2016**, *6*, 2889−2893. (f) Smith, N. E.; Bernskoetter, W. H.; Hazari, N.; Mercado, B. Q. Synthesis and Catalytic Activity of PNP-Supported Iron Complexes with Ancillary Isonitrile Ligands. *Organometallics* **2017**, *36*, 3995−4004. (g) Curley, J. B.; Smith, N. E.; Bernskoetter, W. H.; Hazari, N.; Mercado, B. Q. Catalytic Formic Acid Dehydrogenation and CO_2 Hydrogenation Using Iron PN^RP Pincer Complexes with Isonitrile Ligands. *Organometallics* **2018**, *37*, 3846−3853. (h) Jayarathne, U.; Hazari, N.; Bernskoetter, W. H. Selective Iron-Catalyzed *N*-Formylation of Amines Using Dihydrogen and Carbon Dioxide. *ACS Catal.* **2018**, *8*, 1338−1345.

(10) Nonpincer-type catalysts: (a) Federsel, C.; Boddien, A.; Jackstell, R.; Jennerjahn, R.; Dyson, P. J.; Scopelliti, R.; Laurenczy, G.; Beller, M. A Well-Defined Iron Catalyst for the Reduction of Bicarbonates and Carbon Dioxide to Formates, Alkyl Formates, and Formamides. *Angew. Chem., Int. Ed.* **2010**, *49*, 9777−9780. (b) Ziebart, C.; Federsel, C.; Anbarasan, P.; Jackstell, R.; Baumann, W.; Spannenberg, A.; Beller, M. Well-Defined Iron Catalyst for Improved Hydrogenation of Carbon Dioxide and Bicarbonate. *J. Am. Chem. Soc.* **2012**, *134*, 20701−20704. (c) Bertini, F.; Mellone, I.; Ienco, A.; Peruzzini, M.; Gonsalvi, L. Iron(II) Complexes of the Linear *rac*-Tetraphos-1 Ligand as Efficient Homogeneous Catalysts for Sodium Bicarbonate Hydrogenation and Formic Acid Dehydrogenation. *ACS Catal.* **2015**, *5*, 1254−1265. (d) Zhu, F.; Zhu-Ge, L.; Yang, G.; Zhou, S. Iron-Catalyzed Hydrogenation of Bicarbonates and Carbon Dioxide to Formates. *ChemSusChem* **2015**, *8*, 609−612. (e) Thai, T.-T.; Mérel, D. S.; Poater, A.; Gaillard, S.; Renaud, J.-L. Highly Active Phosphine-Free Bifunctional Iron Complex for Hydrogenation of Bicarbonate and Reductive Amination. *Chem. - Eur. J.* **2015**, *21*, 7066−7070. (f) Fong, H.; Peters, J. C. Hydricity of an Fe-H Species and Catalytic CO_2 Hydrogenation. *Inorg. Chem.* **2015**, *54*, 5124−5135. (g) Coufourier, S.; Gaillard, S.; Clet, G.; Serre, C.; Daturi, M.; Renaud, J.-L. A MOF-Assisted Phosphine Free Bifunctional Iron Complex for the Hydrogenation of Carbon Dioxide, Sodium Bicarbonate and Carbonate to Formate. *Chem. Commun.* **2019**, *55*, 4977−4980. (h) Coufourier, S.; Gaillard, Q. G.; Lohier, J.-F.; Poater, A.; Gaillard, S.; Renaud, J.-L. Hydrogenation of CO_2, Hydrogenocarbonate, and Carbonate to Formate in Water using Phosphine Free Bifunctional Iron Complexes. *ACS Catal.* **2020**, *10*, 2108−2116.

(11) Pincer-type catalysts: (a) Zell, T.; Ben-David, Y.; Milstein, D. Unprecedented Iron-Catalyzed Ester Hydrogenation. Mild, Selective, and Efficient Hydrogenation of Trifluoroacetic Esters to Alcohols Catalyzed by an Iron Pincer Complex. *Angew. Chem., Int. Ed.* **2014**, *53*, 4685−4689. (b) Werkmeister, S.; Junge, K.; Wendt, B.; Alberico, E.; Jiao, H.; Baumann, W.; Jung, H.; Gallou, F.; Beller, M. Hydrogenation of Esters to Alcohols with a Well-Defined Iron Complex. *Angew. Chem., Int. Ed.* **2014**, *53*, 8722−8726. (c) Chakraborty, S.; Dai, H.; Bhattacharya, P.; Fairweather, N. T.; Gibson, M. S.; Krause, J. A.; Guan, H. Iron-Based Catalysts for the Hydrogenation of Esters to Alcohols. *J. Am. Chem. Soc.* **2014**, *136*, 7869−7872. (d) Fairweather, N. T.; Gibson, M. S.; Guan, H. Homogeneous Hydrogenation of Fatty Acid Methyl Esters and Natural Oils under Neat Conditions. *Organometallics* **2015**, *34*, 335−339. (e) Elangovan, S.; Wendt, B.; Topf, C.; Bachmann, S.; Scalone, M.; Spannenberg, A.; Jiao, H.; Baumann, W.; Jung, K.; Beller, M. Improved Second Generation Iron Pincer Complexes for Effective Ester Hydrogenation. *Adv. Synth. Catal.* **2016**, *358*, 820−825. (f) Quintaine, J.; Saudan, L. Hydrogenation of Esters with Fe/Tridentate Ligands Complexes. Patent WO 2015091158 A1.

(12) Nonpincer-type catalysts: Gajewski, P.; Gonzalez-de-Castro, A.; Renom-Carrasco, M.; Piarulli, U.; Gennari, C.; de Vries, J. G.; Lefort, L.; Pignataro, L. Expanding the Catalytic Scope of (Cyclopentadienone) iron Complexes to the Hydrogenation of Activated Esters to Alcohols. *ChemCatChem* **2016**, *8*, 3431−3435.

(13) (a) Garg, J. A.; Chakraborty, S.; Ben-David, Y.; Milstein, D. Unprecedented Iron-Catalyzed Selective Hydrogenation of Activated Amides to Amines and Alcohols. *Chem. Commun.* **2016**, *52*, 5285−5288. (b) Schneck, F.; Assmann, M.; Balmer, M.; Harms, K.; Langer, R. Selective Hydrogenation of Amides to Amines and Alcohols Catalyzed by Improved Iron Pincer Complexes. *Organometallics* **2016**, *35*, 1931−1943. (c) Rezayee, N. M.; Samblanet, D. C.; Sanford, M. S. Iron-Catalyzed Hydrogenation of Amides to Alcohols and Amines. *ACS Catal.* **2016**, *6*, 6377−6383. (d) Jayarathne, U.; Zhang, Y.; Hazari, N.; Bernskoetter, W. H. Selective Iron-Catalyzed Deaminative Hydrogenation of Amides. *Organometallics* **2017**, *36*, 409−416. (e) Artús Suàrez, L.; Jayarathne, U.; Balcells, D.; Bernskoetter, W. H.; Hazari, N.; Jaraiz, M.; Nova, A. Rational Selection of Co-Catalysts for the Deaminative Hydrogenation of Amides. *Chem. Sci.* **2020**, *11*, 2225−2230.

(14) Dong, K.; Elangovan, S.; Sang, R.; Spannenberg, A.; Jackstell, R.; Junge, K.; Li, Y.; Beller, M. Selective Catalytic Two-Step Process for Ethylene Glycol from Carbon Monoxide. *Nat. Commun.* **2016**, *7*, 12075.

(15) (a) Bernskoetter, W. H.; Hazari, N. Hydrogenation and Dehydrogenation Reactions Catalyzed by Iron Pincer Compounds. In *Pincer Compounds: Chemistry and Applications*; Morales-Morales, D., Ed.; Elsevier: Amsterdam, 2018; Chapter 6, pp 111−131. (b) Jones, W. D. Hydrogenation/Dehydrogenation of Unsaturated Bonds with Iron Pincer Catalysis. *Top. Organomet. Chem.* **2019**, *63*, 141−174. (c) Wei, Z.; Jiao, H. Bifunctional Aliphatic PNP Pincer Catalysts for Hydrogenation: Mechanisms and Scope. *Adv. Inorg. Chem.* **2019**, *73*, 323−384.

https://doi.org/10.1021/acs.inorgchem.1c00328
Inorg. Chem. 2021, 60, 6521−6535

(16) (a) Morris, R. H. Iron Group Hydrides in Noyori Bifunctional Catalysis. *Chem. Rec.* **2016**, *16*, 2644−2658. (b) Morris, R. H. Mechanisms of the H_2- and Transfer Hydrogenation of Polar Bonds Catalyzed by Iron Group Hydrides. *Dalton Trans.* **2018**, *47*, 10809−10826. (c) Agbossou-Niedercorn, F.; Michon, C. Bifunctional Homogeneous Catalysts Based on First Row Transition Metals in Asymmetric Hydrogenation. *Coord. Chem. Rev.* **2020**, *425*, 213523.

(17) Recent computational studies by Dub and Gordon show that in solution the concerted H^-/H^+ transfer and dihydrogen activation steps as illustrated in Scheme 1, Catalytic Cycle A, are mechanistically irrelevant. Instead, these reactions proceed in a stepwise fashion. For details, see: (a) Dub, P. A.; Gordon, J. C. The Mechanism of Enantioselective Ketone Reduction with Noyori and Noyori-Ikariya Bifunctional Catalysts. *Dalton Trans.* **2016**, *45*, 6756−6781. (b) Dub, P. A.; Gordon, J. C. Metal-Ligand Bifunctional Catalysis: The "Accepted" Mechanism, the Issue of Concertedness, and the Function of the Ligand in Catalytic Cycles Involving Hydrogen Atoms. *ACS Catal.* **2017**, *7*, 6635−6655.

(18) (a) Chen, X.; Jing, Y.; Yang, X. Unexpected Direct Hydride Transfer Mechanism for the Hydrogenation of Ethyl Acetate to Ethanol Catalyzed by SNS Pincer Ruthenium Complexes. *Chem. - Eur. J.* **2016**, *22*, 1950−1957. (b) Smith, N. E.; Bernskoetter, W. H.; Hazari, N. The Role of Proton Shuttles in the Reversible Activation of Hydrogen via Metal-Ligand Cooperation. *J. Am. Chem. Soc.* **2019**, *141*, 17350−17360.

(19) (a) Bornschein, C.; Werkmeister, S.; Wendt, B.; Jiao, H.; Alberico, E.; Baumann, W.; Junge, H.; Junge, K.; Beller, M. Mild and Selective Hydrogenation of Aromatic and Aliphatic (Di)nitriles with a Well-Defined Iron Pincer Complex. *Nat. Commun.* **2014**, *5*, 4111. (b) Chakraborty, S.; Brennessel, W. W.; Jones, W. D. A Molecular Iron Catalyst for the Acceptorless Dehydrogenation and Hydrogenation of *N*-Heterocycles. *J. Am. Chem. Soc.* **2014**, *136*, 8564−8567.

(20) (a) Otsuka, T.; Ishii, A.; Dub, P. A.; Ikariya, T. Practical Selective Hydrogenation of α-Fluorinated Esters with Bifunctional Pincer-Type Ruthenium(II) Catalysts Leading to Fluorinated Alcohols or Fluoral Hemiacetals. *J. Am. Chem. Soc.* **2013**, *135*, 9600−9603. (b) Dub, P. A.; Henson, N. J.; Martin, R. L.; Gordon, J. C. Unravelling the Mechanism of the Asymmetric Hydrogenation of Acetophenone by [RuX_2(diphosphine)(1,2-diamine)] Catalysts. *J. Am. Chem. Soc.* **2014**, *136*, 3505−3521. (c) Dub, P. A.; Gordon, J. C. The Role of the Metal-Bound N-H Functionality in Noyori-Type Molecular Catalysts. *Nat. Rev. Chem.* **2018**, *2*, 396−408.

(21) (a) Hasanayn, F.; Baroudi, A. Direct H/OR and OR/OR' Metathesis Pathways in Ester Hydrogenation and Transesterification by Milstein's Catalyst. *Organometallics* **2013**, *32*, 2493−2496. (b) Qu, S.; Dai, H.; Dang, Y.; Song, C.; Wang, Z.-X.; Guan, H. Computational Mechanistic Study of Fe-Catalyzed Hydrogenation of Esters to Alcohols: Improving Catalysis by Accelerating Precatalyst Activation with a Lewis Base. *ACS Catal.* **2014**, *4*, 4377−4388. (c) Gusev, D. G. Dehydrogenative Coupling of Ethanol and Ester Hydrogenation Catalyzed by Pincer-Type YNP Complexes. *ACS Catal.* **2016**, *6*, 6967−6981. (d) Gusev, D. G. Rethinking the Dehydrogenative Amide Synthesis. *ACS Catal.* **2017**, *7*, 6656−6662. (e) Gusev, D. G. Revised Mechanisms of the Catalytic Alcohol Dehydrogenation and Ester Reduction with the Milstein PNN Complex of Ruthenium. *Organometallics* **2020**, *39*, 258−270. (f) Tindall, D. J.; Menche, M.; Schelwies, M.; Paciello, R. A.; Schäfer, A.; Comba, P.; Rominger, F.; Hashmi, A. S. K.; Schaub, T. Ru^0 or Ru^{II}: A Study on Stabilizing the "Activated" Form of Ru-PNP Complexes with Additional Phosphine Ligands in Alcohol Dehydrogenation and Ester Hydrogenation. *Inorg. Chem.* **2020**, *59*, 5099−5115.

(22) Dawe, L. N.; Karimzadeh-Younjali, M.; Dai, Z.; Khaskin, E.; Gusev, D. G. The Milstein Bipyridyl PNN Pincer Complex of Ruthenium Becomes a Noyoyi-Type Catalyst under Reducing Conditions. *J. Am. Chem. Soc.* **2020**, *142*, 19510−19522.

(23) For examples of related hydrogenation catalysts based on other transition metals, see: (a) Dub, P. A.; Scott, B. L.; Gordon, J. C. Why Does Alkylation of the N-H Functionality within M/NH Bifunctional Noyori-Type Catalysts Lead to Turnover? *J. Am. Chem. Soc.* **2017**, *139*, 1245−1260. (b) Yuwen, J.; Chakraborty, S.; Brennessel, W. W.; Jones, W. D. Additive-Free Cobalt-Catalyzed Hydrogenation of Esters to Alcohols. *ACS Catal.* **2017**, *7*, 3735−3740.

(24) Zhang, G.; Vasudevan, K. V.; Scott, B. L.; Hanson, S. K. Understanding the Mechanisms of Cobalt-Catalyzed Hydrogenation and Dehydrogenation Reactions. *J. Am. Chem. Soc.* **2013**, *135*, 8668−8681.

(25) Dub, P. A.; Scott, B. L.; Gordon, J. C. Air-Stable NNS (ENENES) Ligands and Their Well-Defined Ruthenium and Iridium Complexes for Molecular Catalysis. *Organometallics* **2015**, *34*, 4464−4479.

(26) (a) Yamamoto, Y. Zerovalent Transition Metal Complexes of Organic Isocyanides. *Coord. Chem. Rev.* **1980**, *32*, 193−233. (b) Boyarskiy, V. P.; Bokach, N. A.; Luzyanin, K. V.; Kukushkin, V. Yu. Metal-Mediated and Metal-Catalyzed Reactions of Isocyanides. *Chem. Rev.* **2015**, *115*, 2698−2779. (c) Barnett, B. R.; Figueroa, J. S. Zero-Valent Isocyanides of Nickel, Palladium and Platinum as Transition Metal σ-Type Lewis Bases. *Chem. Commun.* **2016**, *52*, 13829−13839.

(27) It should be noted that $HN(CH_2CH_2P^iPr_2)_2$ does not always bind to a transition metal in the meridional configuration as one would expect for a pincer ligand. For examples of $HN(CH_2CH_2P^iPr_2)_2$ adopting the facial coordination mode, see: (a) Abdur-Rashid, K.; Graham, T.; Tsang, C.-W.; Chen, X.; Guo, R.; Jia, W.; Amoroso, D.; Sui-Seng, C. Method for the Production of Hydrogen from Ammonia Borane. Patent WO 2008141439 A1. (b) Rozenel, S. S.; Arnold, J. Bimetallic Ruthenium PNP Pincer Complex As a Platform to Model Proposed Intermediates in Dinitrogen Reduction to Ammonia. *Inorg. Chem.* **2012**, *51*, 9730−9739. (c) Fillman, K. L.; Bielinski, E. A.; Schmeier, T. J.; Nesvet, J. C.; Woodruff, T. M.; Pan, C. J.; Takase, M. K.; Hazari, N.; Neidig, M. L. Flexible Binding of PNP Pincer Ligands to Monomeric Iron Complexes. *Inorg. Chem.* **2014**, *53*, 6066−6072.

(28) (a) Marks, T. J.; Kolb, J. R. Covalent Transition Metal, Lanthanide, and Actinide Tetrahydroborate Complexes. *Chem. Rev.* **1977**, *77*, 263−293. (b) Makhaev, V. D. Structural and Dynamic Properties of Tetrahydroborate Complexes. *Russ. Chem. Rev.* **2000**, *69*, 727−746. (c) Besora, M.; Lledós, A. Coordination Modes and Hydride Exchange Dynamics in Transition Metal Tetrahydroborate Complexes. *Struct. Bonding (Berlin)* **2008**, *130*, 149−202.

(29) (a) Custelcean, R.; Jackson, J. E. Dihydrogen Bonding: Structures, Energetics, and Dynamics. *Chem. Rev.* **2001**, *101*, 1963−1980. (b) Belkova, N. V.; Epstein, L. M.; Filippov, O. A.; Shubina, E. S. Hydrogen and Dihydrogen Bonds in the Reactions of Metal Hydrides. *Chem. Rev.* **2016**, *116*, 8545−8587. (c) Golub, I. E.; Filippov, O. A.; Belkova, N. V.; Epstein, L. M.; Rossin, A.; Peruzzini, M.; Shubina, E. S. Two Pathways of Proton Transfer Reaction to (triphos)Cu(η^1-BH_4) *via* a Dihydrogen Bond [triphos = 1,1,1-tris-(diphenylphosphinomethyl)ethane]. *Dalton Trans.* **2016**, *45*, 9127−9135. (d) Belkova, N. V.; Bakhmutova-Albert, E. V.; Gutsul, E. I.; Bakhmutov, V. I.; Golub, I. E.; Filippov, O. A.; Epstein, L. M.; Peruzzini, M.; Rossin, A.; Zanobini, F.; Shubina, E. S. Dihydrogen Bonding in Complex (PP_3)RuH(η^1-BH_4) Featuring Two Proton-Accepting Hydride Sites: Experimental and Theoretical Studies. *Inorg. Chem.* **2014**, *53*, 1080−1090. (e) Golub, I. E.; Gulyaeva, E. S.; Filippov, O. A.; Dyadchenko, V. P.; Belkova, N. V.; Epstein, L. M.; Arkhipov, D. E.; Shubina, E. S. Dihydrogen Bond Intermediated Alcoholysis of Dimethylamine - Borane in Nonaqueous Media. *J. Phys. Chem. A* **2015**, *119*, 3853−3868.

(30) (a) Alberico, E.; Sponholz, P.; Cordes, C.; Nielsen, M.; Drexler, H.-J.; Baumann, W.; Junge, H.; Beller, M. Selective Hydrogen Production from Methanol with a Defined Iron Pincer Catalyst under Mild Conditions. *Angew. Chem., Int. Ed.* **2013**, *52*, 14162−14166. (b) Koehne, I.; Schmeier, T. J.; Bielinski, E. A.; Pan, C. J.; Lagaditis, P. O.; Bernskoetter, W. H.; Takase, M. K.; Würtele, C.; Hazari, N.; Schneider, S. Synthesis and Structure of Six-Coordinate Iron Borohydride Complexes Supported by PNP Ligands. *Inorg. Chem.* **2014**, *53*, 2133−2143.

(31) **1** crystallizes as two independent molecules in the lattice; only molecule A is shown here. **3** has a disordered Cy group; only one

https://doi.org/10.1021/acs.inorgchem.1c00328
Inorg. Chem. 2021, 60, 6521−6535

conformer is shown here. See the Supporting Information for additional information.
(32) In this paper, *cis* and *trans* denote the relationship between the two isocyanide ligands, whereas *syn* and *anti* denote the relationship between the NH hydrogen and the X-type ligand (bromide or hydride).
(33) The ratio between these two isomers can vary slightly from batch to batch.
(34) (a) Wei, D.; Roisnel, T.; Darcel, C.; Clot, E.; Sortais, J.-B. Hydrogenation of Carbonyl Derivatives with a Well-Defined Rhenium Precatalyst. *ChemCatChem* **2017**, *9*, 80−83. (b) Fu, S.; Shao, Z.; Wang, Y.; Liu, Q. Manganese-Catalyzed Upgrading of Ethanol into 1-Butanol. *J. Am. Chem. Soc.* **2017**, *139*, 11941−11948. (c) Wellala, N. P. N.; Luebking, J. D.; Krause, J. A.; Guan, H. Roles of Hydrogen Bonding in Proton Transfer to $\kappa^P,\kappa^N,\kappa^P$-N$(CH_2CH_2P^iPr_2)_2$-Ligated Nickel Pincer Complexes. *ACS Omega* **2018**, *3*, 4986−5001.
(35) Ogata, O.; Nakayama, Y.; Nara, H.; Fujiwhara, M.; Kayaki, Y. Atmospheric Hydrogenation of Esters Catalyzed by PNP-Ruthenium Complexes with an *N*-Heterocyclic Carbene Ligand. *Org. Lett.* **2016**, *18*, 3894−3897.
(36) One *tert*-butyl group is disordered and was refined with a two-component disorder model. Only the major component is shown here. The cocrystallized half-molecule of toluene is also disordered. See the Supporting Information for additional information.
(37) One *tert*-butyl group is disordered and was refined with a two-component disorder model. Only the major component is shown here. See the Supporting Information for additional information.
(38) Mironov, M. A. General Aspects of Isocyanide Reactivity. In *Isocyanide Chemistry: Applications in Synthesis and Material Science*, 1st ed.; Nenajdenko, V. G., Ed.; Wiley-VCH: Weinheim, Germany, 2012; pp 35−73.
(39) Goldman, A. S.; Krogh-Jespersen, K. Why Do Cationic Carbon Monoxide Complexes Have High C-O Stretching Force Constants and Short C-O Bonds? Electrostatic Effects, Not σ-Bonding. *J. Am. Chem. Soc.* **1996**, *118*, 12159−12166.
(40) Similar results were obtained when benzene or THF was used as the solvent for extraction.
(41) Rautenstrauch, V.; Hoang-Cong, X.; Churlaud, R.; Abdur-Rashid, K.; Morris, R. H. Hydrogenation versus Transfer Hydrogenation of Ketones: Two Established Ruthenium Systems Catalyze Both. *Chem. - Eur. J.* **2003**, *9*, 4954−4967.
(42) *cis,anti*-**7′** crystallizes as two independent molecules with one water molecule in the lattice. Each molecule has one disordered *tert*-butyl group, which was refined as a two-component disorder model. Only the major component of one molecule is shown here. See the Supporting Information for additional information.
(43) Dub, P. A.; Batrice, R. J.; Gordon, J. C.; Scott, B. L.; Minko, Y.; Schmidt, J. G.; Williams, R. F. Engineering Catalysts for Selective Ester Hydrogenation. *Org. Process Res. Dev.* **2020**, *24*, 415−442.
(44) Babij, N. R.; McCusker, E. O.; Whiteker, G. T.; Canturk, B.; Choy, N.; Creemer, L. C.; DeAmicis, C. V.; Hewlett, N. M.; Johnson, P. L.; Knobelsdorf, J. A.; Li, F.; Lorsbach, B. A.; Nugent, B. M.; Ryan, S. J.; Smith, M. R.; Yang, Q. NMR Chemical Shifts of Trace Impurities: Industrially Preferred Solvents Used in Process and Green Chemistry. *Org. Process Res. Dev.* **2016**, *20*, 661−667.
(45) (a) Clarke, Z. E.; Maragh, P. T.; Dasgupta, T. P.; Gusev, D. G.; Lough, A. J.; Abdur-Rashid, K. A Family of Active Iridium Catalysts for Transfer Hydrogenation of Ketones. *Organometallics* **2006**, *25*, 4113−4117. (b) Bertoli, M.; Choualeb, A.; Gusev, D. G.; Lough, A. J.; Major, Q.; Moore, B. PNP Pincer Osmium Polyhydrides for Catalytic Dehydrogenation of Primary Alcohols. *Dalton Trans.* **2011**, *40*, 8941−8949.
(46) Ma, W.; Cui, S.; Sun, H.; Tang, W.; Xue, D.; Li, C.; Fan, J.; Xiao, J.; Wang, C. Iron-Catalyzed Alkylation of Nitriles with Alcohols. *Chem. - Eur. J.* **2018**, *24*, 13118−13123.

https://doi.org/10.1021/acs.inorgchem.1c00328
Inorg. Chem. 2021, 60, 6521−6535